

1  
2  
3  
4  
5  
6  
7  
8  
9  
10  
11  
12  
13  
14  
15  
16  
17  
18  
19  
20  
21  
22  
23  
24  
25  
26  
27  
28  
29

# **A review on the modelling of wave-structure interactions based on OpenFOAM**

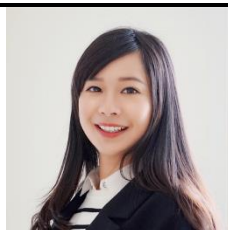
**Abstract:** The modelling of wave-structure interaction (WSI) has significant applications in understanding natural processes as well as securing the safety and efficiency of marine engineering. Based on the technique of Computational Fluid Dynamics (CFD) and the open-source simulation framework - OpenFOAM, this paper provides a state-of-the-art review of WSI modelling methods. The review categorises WSI scenarios and suggests their suitable computational approaches, concerning a rigid, deformable or porous structure in regular, irregular, non-breaking or breaking waves. Extensions of WSI modelling for wave-structure-seabed interactions and various wave energy converters are also introduced. As a result, the present review aims to help understand the CFD modelling of WSI and guide the use of OpenFOAM for target WSI problems.

**Keywords:** Wave-structure interaction; Computational Fluid Dynamics; OpenFOAM.

## Authors



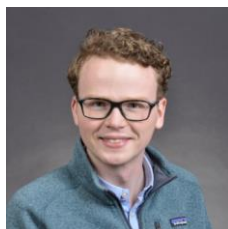
**Dr Luofeng Huang**  
Assistant Professor  
Cranfield University,  
UK, [luofeng.huang@cranfield.ac.uk](mailto:luofeng.huang@cranfield.ac.uk)



**Dr Yuzhu Li**  
Assistant Professor  
National University of  
Singapore, Singapore  
[pearl.li@nus.edu.sg](mailto:pearl.li@nus.edu.sg)



**Dr Daniela Benites**  
PhD Graduate  
University College  
London, UK  
[ucemben@ucl.ac.uk](mailto:ucemben@ucl.ac.uk)



**Dr Christian Windt**  
Postdoc  
TU Braunschweig,  
Germany, [c.windt@tu-braunschweig.de](mailto:c.windt@tu-braunschweig.de)



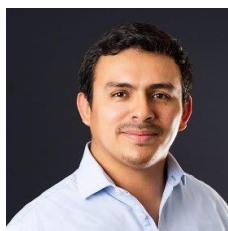
**Dr Anna Feichtner**  
PhD Graduate  
University of Exeter,  
UK  
[af506@exeter.ac.uk](mailto:af506@exeter.ac.uk)



**Dr Sasan Tavakoli**  
Postdoc  
Aalto University,  
Finland  
[sasan.tavakoli@aalto.fi](mailto:sasan.tavakoli@aalto.fi)



**Dr Josh Davidson**  
Assistant Professor  
TU Budapest,  
Hungary, [davidson@ara.bme.hu](mailto:davidson@ara.bme.hu)



**Prof Ruben Paredes**  
Full Professor  
ESPOL University,  
Ecuador  
[rparedes@espol.edu.ec](mailto:rparedes@espol.edu.ec)



**Ms Tadea Quintuna**  
Master Student  
University of Liège  
Belgium, [mariatadeaqr.mtqa@gmail.com](mailto:mariatadeaqr.mtqa@gmail.com)



**Dr Edward Ransley**  
Senior Research Fellow  
University of Plymouth,  
UK, [edward.ransley@plymouth.ac.uk](mailto:edward.ransley@plymouth.ac.uk)



**Dr Marco Colombo**  
Assistant Professor  
University of Sheffield,  
UK, [m.colombo@sheffield.ac.uk](mailto:m.colombo@sheffield.ac.uk)



**Mr Minghao Li**  
CFD Engineer  
TU Chalmers,  
Sweden, [lmhao1014@hotmail.com](mailto:lmhao1014@hotmail.com)



**Dr Philip Cardiff**  
Associate Professor  
University College  
Dublin, Ireland  
[philip.cardiff@ucd.ie](mailto:philip.cardiff@ucd.ie)



**Prof Gavin Tabor**  
Full Professor  
University of Exeter,  
UK  
[g.r.tabor@exeter.ac.uk](mailto:g.r.tabor@exeter.ac.uk)

## 30 **1. Introduction**

### 31 **1.1 Background**

32 Wave-Structure Interaction (WSI) is defined as ocean waves applying forces to one or multiple  
33 solid bodies and the solid's dynamic response changes the surrounding wave field  
34 simultaneously. WSI processes are ubiquitous in both marine environment and engineering, e.g.  
35 influencing the distribution of sea ice and vegetation, and dictating the safety and performance  
36 of ships and offshore installations. Thereby, the modelling of WSI is of great importance for  
37 marine science, design and operations.

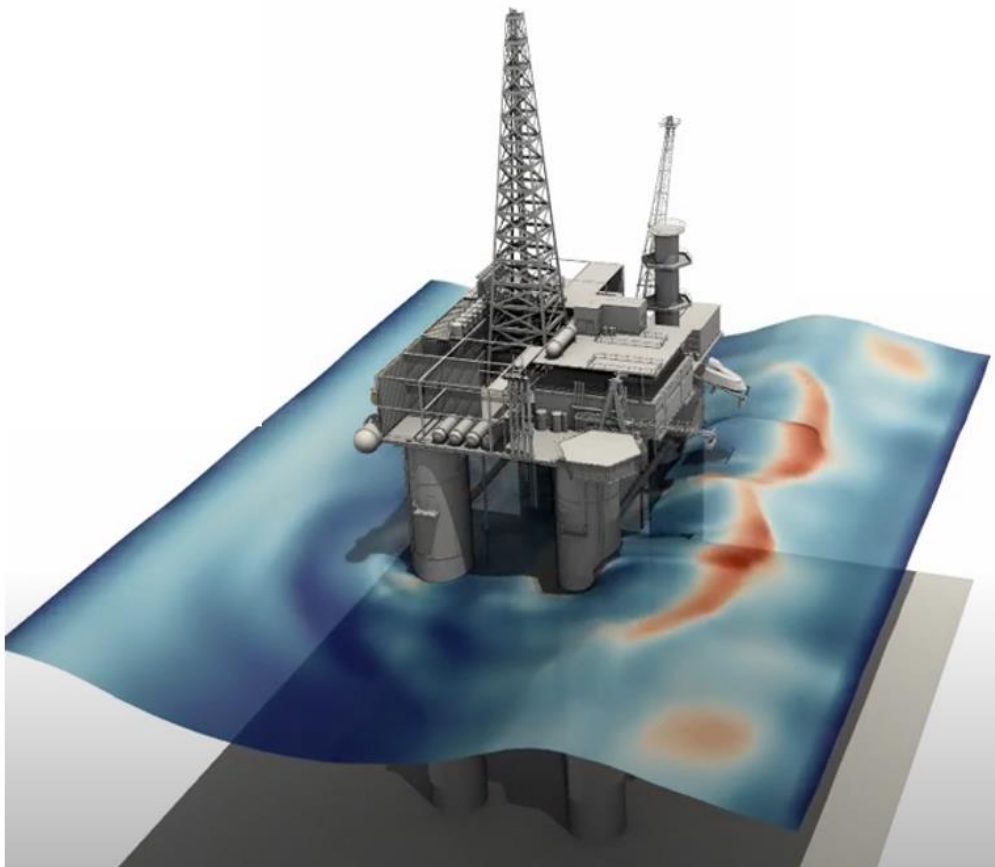
38 WSI modelling has been categorised into one-way coupling and two-way coupling. In one-way  
39 coupling, the fluid impacts the structure, but not the other way around. In two-way coupling  
40 models, the fluid and the structure impact each other. The modelling started with analytical  
41 approaches. Initially, mathematical equations were developed to describe ocean waves as a  
42 periodic movement along a timeline. Those wave equations were used to calculate the harmonic  
43 wave loads on a structure, or wave-induced structural motions. Subsequently, the wave  
44 diffraction by a structure was also formulated. Such analytical solutions for WSI have been  
45 developed since the early 20<sup>th</sup> century and approached a degree of maturity around the 1990s,  
46 with a wide range of problems addressed by the Morison equation and the potential flow theory  
47 coupled with structural solutions [1–5]. However, most analytical WSI works were limited to  
48 linear wave conditions and inviscid fluids to obtain closed-form solutions, only valid for small-  
49 amplitude waves.

50 Since the 2000s, nonlinear wave modelling has become popular using the potential flow theory  
51 in combination with higher-order Boundary Element Methods (BEM). This BEM approach  
52 allows the prediction of high-steepness waves and the corresponding response of structures,  
53 which has shown good accuracy against experiments so long as the wave does not break by  
54 itself or by the structure [6,7]. However, the BEM approach is based upon dimensionality  
55 reduction as the discretisation is applied on a boundary rather than on a volume. This limits the  
56 applicable structures to simple geometries, such as a cuboid, a cylinder or a sphere. Overall, the  
57 BEM approach still cannot model WSI phenomena that involve strong nonlinearities.

58 With the advances in modern computational techniques, computational fluid dynamics (CFD)  
59 models have been developed to address more realistic WSI problems. In CFD, the physical  
60 domain is represented by a corresponding computational domain, in which a solid geometry  
61 can be inserted. The space between the surface of the structure and the domain boundaries is  
62 the fluid field, which can be discretised and use the Navier-Stokes equations to obtain highly-  
63 nonlinear wave profiles.

64 There are two main branches of CFD, mesh-free methods and mesh-based methods. The  
65 computational speed has been a significant challenge for mesh-free methods, such as the  
66 Smoothed Particle Hydrodynamics (SPH), which represents the fluid and structure as particles,  
67 e.g. [8]. In addition, in SPH it is hard to develop boundary conditions such as inlet/outlet and  
68 the method requires artificial inputs for viscous effects [9]. These are significant challenges for  
69 WSI modelling, in which inlet/outlet and fluid viscosity are essential. Thus the WSI  
70 applicability of mesh-free methods is limited.

71 In terms of mesh-based methods of CFD, for example the Finite Volume Method (FVM), the  
72 solid geometry is modelled as a closed surface that is in contact with numerous computational  
73 cells to represent its structural complexity. In addition, a specific boundary-layer mesh can be  
74 built around the geometry to account for fluids' boundary-layer effect. Local mesh refinements  
75 are mature with FVM. These features render mesh-based CFD a suitable approach to model  
76 and analysing WSI problems, with the level of fidelity sufficiently high that the simulation can  
77 closely reproduce what happens in real sea states (See Figure 1 for an example).



78

79 Figure 1: CFD simulation example of waves interacting with a realistic structure [10]

80

## 81 **1.2 Choices of CFD software**

82 Different software is available for WSI simulations, ranging from commercial and open-source  
83 software to in-house developments. Commercial tools commonly feature graphical user  
84 interfaces (GUIs) and often specific numerical methods, e.g. for multi-physics analysis.  
85 However, the often significant license fees and, to some extent, the restricted access to the  
86 source code, possibly hinders the usage of commercial software for WSI applications.

87 By avoiding license fees and providing access to source code, open-source CFD software has  
88 gained popularity and is commonly backed by active communities. For OpenFOAM, dedicated  
89 workshops and user group meetings facilitate knowledge exchange within the community,  
90 driving new developments. In addition, a few private companies, such as Engys or WIKKI, are  
91 heavily involved in code development. Drawbacks of using open-source software may arise  
92 from steep learning curves for beginners. Furthermore, developments of new (advanced)  
93 numerical tools lack profit as a motivator. However, unlimited access to the source code enables  
94 custom code development, facilitating the open-source software to be applied in a wide range  
95 of applications. Apart from OpenFOAM, there is also other open-source software that has made  
96 significant contributions to WSI modelling, such as REEF3D and Gerris [11,12].

97 In-house codes are either driven by specific (physical) problems or the desire to include  
98 advanced numerical algorithms. Their nature makes them unavailable to a large community.  
99 Examples of such codes can be found in [13,14].

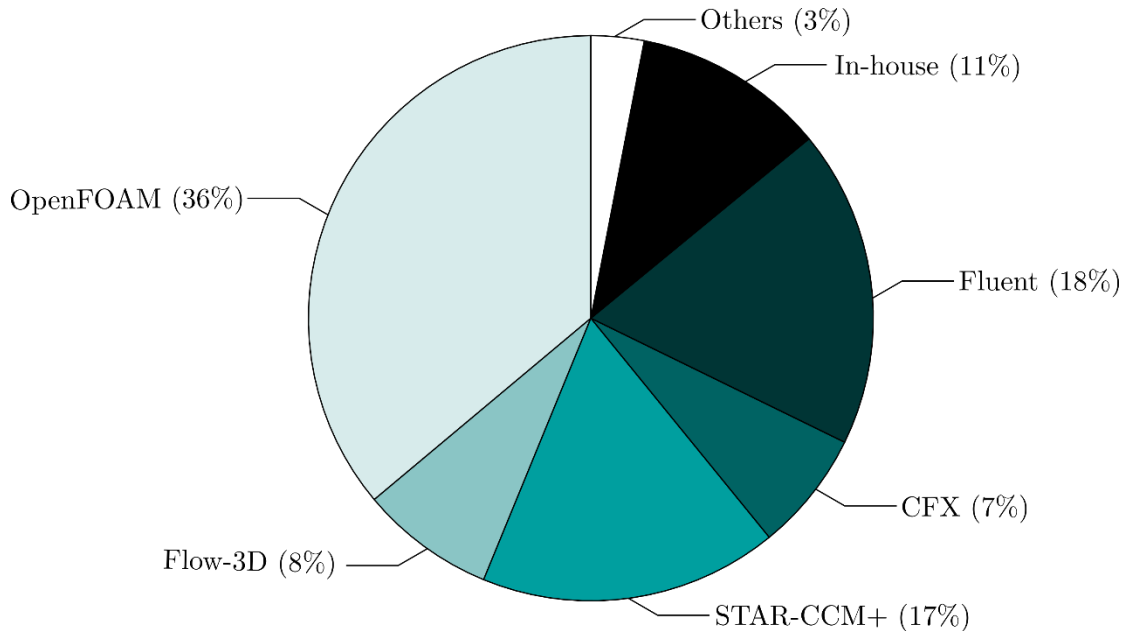
100 The wide range of different CFD software suites raises the question of which one to select.  
101 Decision drivers of choosing a specific CFD software for WSI are diverse, often being the  
102 available turbulence models or numerical wave generation and absorption. Additional decision  
103 drivers may include project time frame, budget, and user experience.

104 In principle, there is not a function that is implemented in commercial software that cannot be  
105 implemented in OpenFOAM, and vice versa. The main differences, on one hand, include that  
106 OpenFOAM enables more possibilities for learning and research purposes, as it is completely  
107 free to view and develop the code. On the other hand, the learning curve for OpenFOAM is  
108 known to be longer than commercial software, making it more challenging for a beginner who  
109 may have limited time for a specific project.

110 Some studies can be found which perform comparative analyses of different CFD software.  
111 Based on the analysis of extreme wave loading, Westphalen et al. [15] consider STAR-CCM+,  
112 ANSYS CFX, the in-house Cartesian cut-cell solver AMAZON-SC 3D, and an SPH solver.  
113 Sjökvist et al. [16,17] present a comparison of OpenFOAM with ANSYS Fluent. Most recently,  
114 the CCP-WSI Blind Test Series 1-3 [17–19] aimed at delivering comprehensive code-to-code

115 and code-to-experiment comparisons of different modelling approaches and dedicated  
116 experimental validation data. By way of example, Figure 2 shows the CFD software used for  
117 WSI simulations of Wave Energy Converters (WECs) and their relative popularity in the  
118 literature.

119



120

121 Figure 2: CFD software used for WSI simulations of WECs and their relative popularity  
122 among approximately 200 reviewed studies [21].

123

### 124 1.3 Scope of this paper

125 Although CFD simulations have been shown capable of modelling WSI, the quality of the  
126 simulations is dependent on the user's computational setups. The capabilities of CFD provide  
127 abundant options on numerical models and setups to account for the free surface, wave  
128 modelling, turbulence effect, and structural response, among others. When inappropriate setups  
129 are used, simulations can crash or lead to unphysical/erroneous results. For this reason, review  
130 articles can bring significant contributions by helping users understand CFD and providing  
131 recommendations on suitable modelling branches for specific problems.

132 In order to provide a comprehensive review of CFD modelling of WSI problems, the present  
133 work selects OpenFOAM as the framework. Based on the open-source code, primary WSI  
134 modelling approaches are reviewed and their applicability and limitation for various physical  
135 problems are discussed. This allows readers to refer to corresponding source code, gaining a  
136 deeper understanding than appreciating black-box functions in commercial CFD tools.

137 The remainder of this paper is organised as follows: Section 2 introduces relevant fluid  
 138 modelling approaches, i.e. modelling different types of ocean surface waves. Section 3 reviews  
 139 WSI modelling concerning various structural characteristics, for (3.1) rigid fixed structures,  
 140 (3.2) rigid floating structures, (3.3) deformable structures, (3.4) porous structures; furthermore,  
 141 (3.5) provides an extension of WSI modelling that couples with seabed response. Section 4  
 142 presents the modelling of various types of WECs, where the modelling methods of mooring  
 143 lines and power-take-off systems are also introduced. Finally, Section 5 summarises this work  
 144 with its main conclusions.

145

## 146 2. Wave flow

### 147 2.1 Free surface modelling

148 A key requirement for simulating water waves in OpenFOAM is modelling the evolving free  
 149 surface interface. The most popular method for achieving this is the Volume of Fluid (VOF)  
 150 approach, detailed in Section 2.1.1, which can simulate complex WSI problems such as those  
 151 involving wave breaking, overtopping and slamming. Alternative methods are also available,  
 152 as discussed in Section 2.1.2. These methods are not widely applicable as VOF but can be  
 153 capable of modelling a restricted range of WSI conditions with potential computational savings.

154

#### 155 2.1.1 The VOF method

156 The VOF method tracks the relative volumetric percentage of different fluids in each cell. For  
 157 the case of wave simulations, the VOF method typically considers two fluid phases: water and  
 158 air. This is depicted in Figure 3(a), where the volume fraction of water is displayed - a value of  
 159 1 corresponds to a cell containing 100% water, a value of 0 corresponds cells with 100% air,  
 160 and a value between 0 and 1 represent the cells around the free surface interface.

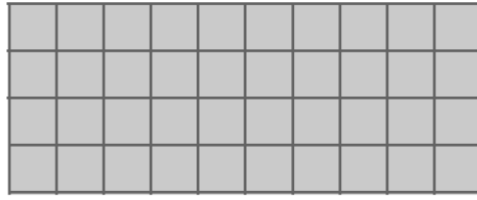
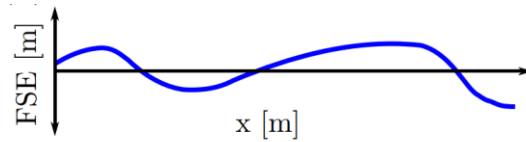
161

0	0	0	0	0	0	0	0	0	0	0	0	0	0	0	0	0	0	0	0	0
0	0	0	0	0	0	0	0	0	0	0	0	0	0	0	0	0	0	0	0	0
0	0	0	0	0	0	0	0	0	0	0	0	0	0	0	0	0	0	0	0	0
0.37	0.86	0.42	0.01	0	0	0	0	0	0	0.04	0.41	0.89	1	1	0.98	0.97	0	0	0	0
1	1	1	0.88	0.13	0.01	0.03	0.21	0.56	0.97	1	1	1	1	0.97	0.02	0	0	0	0	0
1	1	1	1	1	0.97	0.99	1	1	1	1	1	1	1	1	1	0.79	0.34	0.05	0.01	0
1	1	1	1	1	1	1	1	1	1	1	1	1	1	1	1	1	1	1	1	1
1	1	1	1	1	1	1	1	1	1	1	1	1	1	1	1	1	1	1	1	1
1	1	1	1	1	1	1	1	1	1	1	1	1	1	1	1	1	1	1	1	1

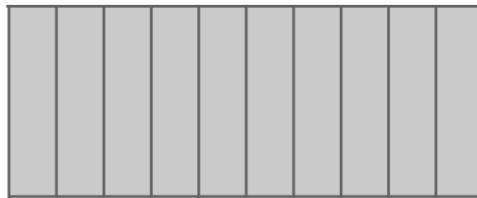
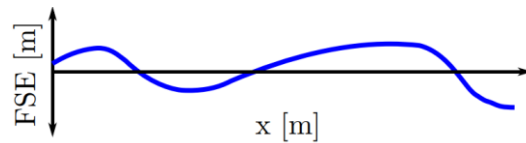
162

163

(a) *interFoam* and *interIsoFoam* (The VOF method)



(b) *potentialFreeSurfaceFoam*



(c) *shallowWaterFoam*

Figure 3: Depiction of the methodologies of different OpenFOAM solvers for free-surface flow [22].

164

165

166

167

168

169

170

171 The most commonly used OpenFOAM solver for wave modelling is *interFoam*, which  
 172 considers two fluid phases (air and water) and that the fluids are incompressible, immiscible,  
 173 and viscous. However, other solvers, shown in Figure 3, might be more efficient for specific  
 174 cases e.g. simulating an oil spill [23], or to include air compressibility e.g. calculating wave  
 175 impact/slamming loads [24–26] and simulating an oscillating-water-column WEC [27,28]. In  
 176 addition, it is possible to decrease the complexity of the model by neglecting the effect of  
 177 viscosity e.g. to reduce the computational burden of fully resolving the boundary layers [29].

178 A variant of the *interFoam* solver, *interIsoFoam*, has been developed and is gaining popularity  
 179 due to its improved ability to handle the free surface interface. The *interIsoFoam* solver  
 180 employs the novel geometric VOF algorithm, *isoAdvector* [30], which maintains a sharp  
 181 interface by constructing and advecting an isosurface inside the cells around the interface  
 182 position. By contrast, the original *interFoam* solver utilises the multi-dimensional limiter for  
 183 explicit solution (MULES) method, which employs an artificial compression velocity term to  
 184 bound the interface [31]. Considering wave propagation, *interIsoFoam* has been shown to  
 185 maintain a sharper interface than *interFoam* [32] and significantly reduce the excessive wave



186 dissipation inherent in traditional VOF methods [33], despite the considerably higher  
187 computational cost.

188 To tackle the spurious velocities and, thus, allow larger time steps and better performance of  
189 turbulence models at the interface, recently, the Ghost Fluid Method (GFM) has been  
190 implemented within OpenFOAM [34]. The GFM ensures a continuous velocity field across the  
191 interface by coupling the two phases (high and low density) via specific jump conditions at the  
192 interface.

193 In a comparative study, Peltonen et al. [35] investigated the performance of the GFM (based on  
194 [34]) and the traditional VOF for a number of marine-related test cases, i.e. two-dimensional  
195 inviscid flow over a step, two-dimensional interface shear layer, and ship wave generation for  
196 a Wigley hull and the Hamburg test case. The authors found rather subtle differences for the  
197 specific test cases and suggest a further improvement by coupling GFM with geometric  
198 interface capturing methods, such as *isoAdvector*.

199 Recently, MULES has been improved with the Piecewise-Linear Interface Calculation (PLIC)  
200 and Multicut PLIC (MPLIC) [36]. PLIC represents an interface by surface cuts that split each  
201 cell to match the volume fraction of the phase in that cell. The surface cuts are oriented  
202 according to the point field of the local phase fraction. The phase fraction on each cell face, i.e.  
203 the interpolated value, is then calculated from the amount submerged below the surface cut.  
204 MPLIC is for handling multiple surface cuts, where a single cut in one cell is insufficient, e.g.  
205 the water volume in one cell is between two separated air volumes. PLIC and MPLIC thus have  
206 improved the modelling of interface/free surface, e.g. achieved high-resolution modelling of  
207 water splash [37].

208

### 209 2.1.2 Alternative methods

210 Schmitt et al. [22] explored the choice of solvers in OpenFOAM other than those based on the  
211 VOF method, which could be utilised to implement numerical wave tanks, namely:  
212 *potentialFreeSurfaceFoam* and *shallowWaterFoam*. While hundreds of publications have  
213 utilised the VOF method for WSI, Schmitt et al. [22] found that less than a dozen have used  
214 *shallowWaterFoam* and only two have used *potentialFreeSurfaceFoam*.

215 The *potentialFreeSurfaceFoam* solver is a single-phase solver, as depicted in Figure 3(b), that  
216 calculates the free surface as a single-valued function, thus cannot simulate effects such as wave  
217 breaking. *PotentialFreeSurfaceFoam* is based on the *pimpleFoam* solver, which is widely used  
218 in a broad range of applications for incompressible, single-phase, transient flows. A special  
219 boundary condition is added to the *pimpleFoam* solver, called *waveSurfacePressure*, which

220 calculates the change in surface elevation at each time step based on the volume flux for the  
221 cells at the top boundary. The *shallowWaterFoam* solver employs simplified equations that are  
222 valid in shallow water conditions. The shallow water equations [38] enable the velocity to be  
223 represented by a depth-averaged horizontal component, eliminating the requirement to solve  
224 for the vertical direction. Therefore, massive reductions in the overall cell count are achieved  
225 since the domain only needs to be discretised using one cell in the vertical direction, as depicted  
226 in Figure 3(c). The shallow water equations only consider the water phase, thus  
227 *shallowWaterFoam* is a single-phase solver, where the surface elevation is directly available as  
228 a simulation variable. Another alternative solver is *interTrackFoam*, which applies an interface  
229 tracking that considers single-phase by enforcing the free surface boundary conditions on it  
230 [39]. However, this method is not applicable in a situation where the water can be discontinuous  
231 due to the structure, e.g. waves bring partial water to go on top of a structure [40], because in  
232 this scenario the free surface is no longer a continuous boundary. More examples of using  
233 alternative models to VOF can be found in Schmitt et al. [22].

234

## 235 **2.2 Wave modelling**

### 236 2.2.1 Variety of waves

237 There are a variety of wave theories that can be used to generate progressive ocean surface  
238 waves. The waves can be divided into regular (linear and nonlinear), irregular waves and  
239 focussed waves. In this sub-section, the implementation of different wave theories in  
240 OpenFOAM will be introduced.

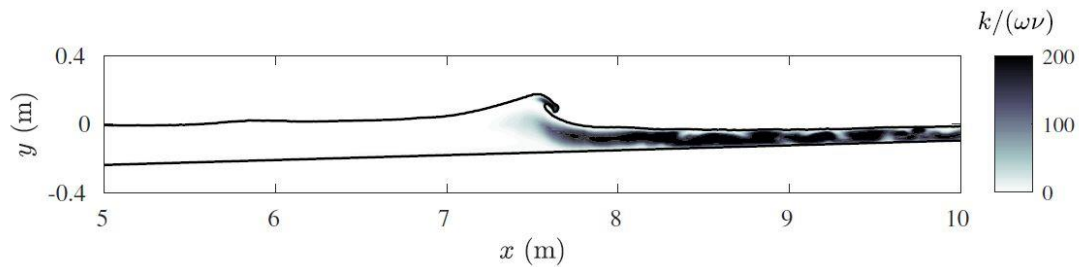
241 For regular wave modelling the incident waves are periodic. To represent more realistic wave  
242 conditions, various regular waves of different wave heights and frequencies can propagate in a  
243 certain region, known as irregular waves (also sometimes called random waves). The spectrum  
244 of irregular waves can be obtained through on-site measurements and inputted into simulations.  
245 Commonly used wave spectra include the JONSWAP, the Pierson-Moskowitz and the  
246 Bretschneider types [41,42], in which JONSWAP is considered the most widely used.

247 Focussed waves are normally considered when assessing extreme wave loads, where a single  
248 high-crest wave is formed due to the accumulation of wave components (although there are  
249 also trough-focussed or focussed at any particular phase). The focussed crest waves are  
250 normally formed through the delicate superposition of multiple wave peaks.

251 When the water waves approach the coast, the water depth decreases to shallow enough that  
252 the wave may feel the presence of seabed and change its shape. This action induces increasing  
253 wave height and decreasing wavelength, which will cause the wave to break at a certain point.

254 This process is known as surf zone breaking waves, shown in Figure 4. The bathymetry will  
255 influence the wave breaking type from spilling, plunging, collapsing, or surging. The modelling  
256 of breaking waves is different from modelling non-breaking surface waves (for non-breaking  
257 waves potential-flow theory or a laminar model can be used).

258



259

260 Figure 4: Plunging-type breaking wave simulation [43], where  $k/(\omega\nu)$  indicates the turbulence  
261 level.

262

263 In the deep-water regime of offshore/coastal regions, where the surface wave is not influenced  
264 by seabed, breaking waves can also occur due to the instability of wave trains subject to initially  
265 small perturbations. The resonant interaction between the carrier wave trains and the small  
266 perturbations can lead to an exponential growth of the wave amplitudes for the side bands, and  
267 further wave breaking. A study by Li and Fuhrman [44] simulated the so-called Class I  
268 (Benjamin-Feir instability) and Class II (crescent waves) deep-water wave instabilities  
269 involving wave breaking with the Reynolds stress turbulence model. Figure 5 shows the three-  
270 dimensional wave breaking evolved from crescent waves.

271

272

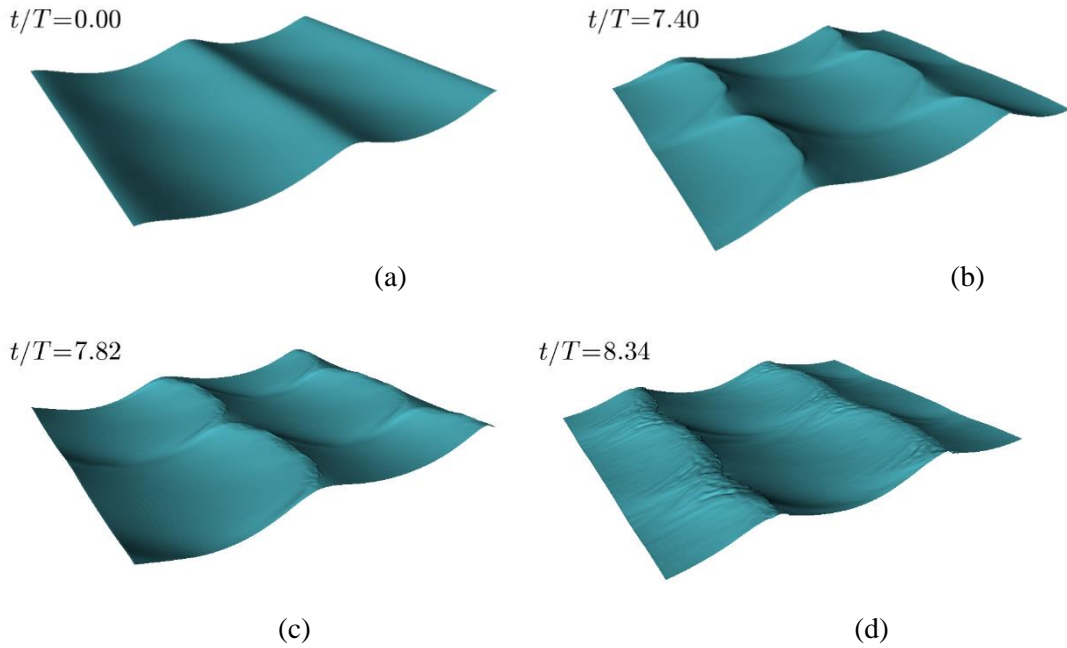
273

274

275

276

277



278  
279

280  
281

282 Figure 5: Free surface evolution during the interaction between a plane wave train and three-  
283 dimensional perturbations: (a) the initial 2D wave train (b) 3D crescent waves (c) wave  
284 breaking on the crescent crests (d) disturbed free surface during wave breaking [44].

285

286 In open seas, focussed wave groups can also form breaking waves. Resulting from the  
287 superposition of multiple waves or a storm, such rogue waves can be formed as a random event  
288 [45]. Bredmose and Jacobsen [46] modelled breaking waves generated from focused wave  
289 groups using the *interFoam* solver and investigated the breaking wave interaction with an  
290 offshore wind turbine foundation in the intermediate water. As strong turbulence is produced  
291 in wave breaking, this will require turbulence modelling that will be discussed in Section 2.2.3.

292

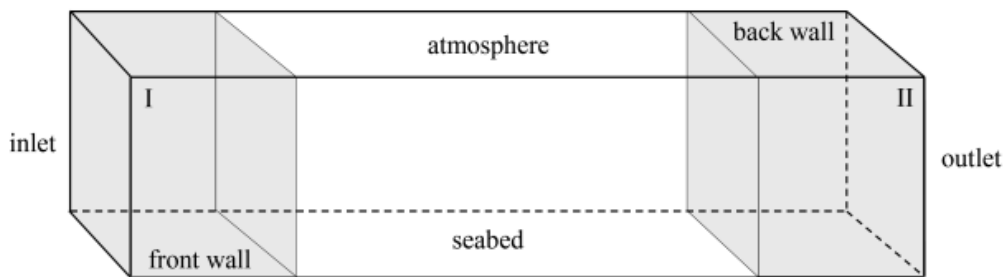
### 293 2.2.2 Wave generation and absorption in OpenFOAM

294 To model waves numerically, it is essential to consider the generation of the desired wave at  
295 the inlet of the Numerical Wave Tank (NWT) and the absorption at the outlet to avoid reflected  
296 waves. Numerical wavemakers can be implemented by different methods, namely: (a)  
297 including a physically similar wave generator/paddle by making the inlet boundary move - this  
298 method is similar to wave tank experiments [47,48]; (b) implementing dictating functions to  
299 force the CFD solutions to present a target wave condition, where the relaxation method and  
300 the static boundary method are two of the maturest [49,50]. For (a), additional boundary  
301 condition modifications and dynamic mesh treatment are required, therefore (b) is the typical  
302 approach is NWT modelling.

303 In the case of the relaxation technique, the generation of the wave is initialised by using the  
 304 analytical solution of the wave theory applied in the inlet zone. Normally the solutions are also  
 305 artificially changed in the outlet zone to absorb the wave thus modelling a far-field condition,  
 306 as shown in Figure 6(a). This method has been implemented in a toolbox named *waves2Foam*  
 307 [51].

308 In the relaxation approach, a user-defined function is introduced to modify the solution of a  
 309 computational variable  $\xi$  (e.g. velocity or volume fraction of water) of each timestep by  
 310 blending a target value, as  $\xi = \chi \xi_{computed} + (1 - \chi) \xi_{target}$ , where  $\chi$  is the relaxation  
 311 coefficient taking values between 0 and 1, as shown in Figure 6(b). With this method applied,  
 312 theoretical target waves are forced at the inlet and outlet boundaries (where  $\chi = 0$ ) and  
 313 unmodified computed results are obtained in the middle of the NWT, where  $\chi = 1$ , with the inlet  
 314 and outlet zones gradually changing  $\chi$  to relax the solution change. The relaxation technique  
 315 has been proven effective and stable, mostly able to generate and absorb waves with negligible  
 316 error [52–54]. Nonetheless, the size of the computational domain tends to increase due to  
 317 adding the relaxation zones.

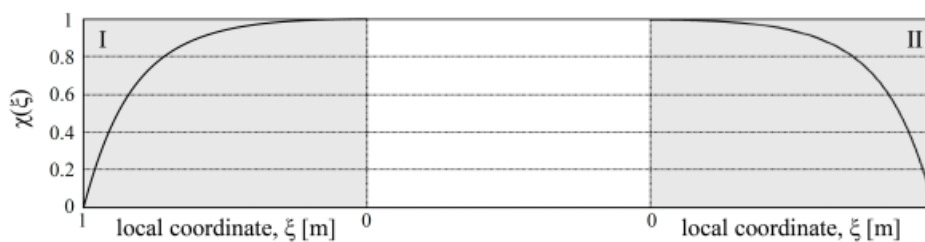
318



319

(a) Inlet and outlet relaxation zones (grey) in a numerical wave tank

320



321

(b) The value of the spatial weighting factor

322

323 Figure 6: Illustration of the relaxation method [55].

323

324

325 As an alternative, the static boundary method that uses boundary conditions to control the  
 326 generated wave was developed, and it is available in OpenFOAM as *IHFoam* and *olaFlow*

327 [10,56]. At the wave generation boundary, the boundary conditions are obtained from wave  
328 theory. For the absorption boundary, a correction velocity is applied to cancel out the incoming  
329 waves. This method has also been successfully used across the WSI community [57–59], and  
330 further information on the developer’s toolbox can be found in [51,60,61].

331 Compared to the relaxation method, the static boundary method can avoid the use of relaxation  
332 zones that increases the computational cost. Nonetheless, it has been highlighted that wave  
333 absorption using the static boundary method is a challenge. The wave field near the outlet  
334 boundary is normally disturbed by a structure, i.e. it is not pre-known as an incident wave field,  
335 so measuring the flow before the outlet is essential for the cancelling out. However, the  
336 measured flow near the outlet is a combination of incident and reflected wave, which means  
337 wave filters must be used to derive a cancelling-out wave train from the outlet. The wave  
338 filtering technique strongly relies on wave theories. Previously, this approach was only valid  
339 for linear wave theory in shallow water [62]. Further development has been made by Higuera  
340 [63] to enable the absorption of deep waters, but the author still highlighted the incapability of  
341 absorbing nonlinear waves. Recently, Borsboom and Jacobsen [64] have made an advancement  
342 by analytically decomposing the measured flow into multiple modes. This significantly  
343 improved the absorption of nonlinear waves and the undesired reflection was reported to be  
344 less than 5% of the incident waves.

345 Windt et al. [65] used different test cases to assess available OpenFOAM methods for numerical  
346 wave tanks. Their comparison suggested that the static boundary method is the most  
347 computationally efficient for wave generation, while the wave absorption part may be better  
348 replaced by using a numerical beach method, which is implemented as a dissipating region  
349 nearby the outlet.

350 For either the relaxation method or the static boundary method, it is worthwhile to note that at  
351 least 10 cells per wave height and 100 cells per wavelength should be used to generate an  
352 accurate target wave. This mesh density generally gives a deviation of less than 1% against  
353 theoretical waves, provided that other setups are reasonable [66]. More information on the  
354 different wave generation methodologies can be found in the reviews of Schmitt and Elsaesser  
355 [67], and Windt et al. [68].

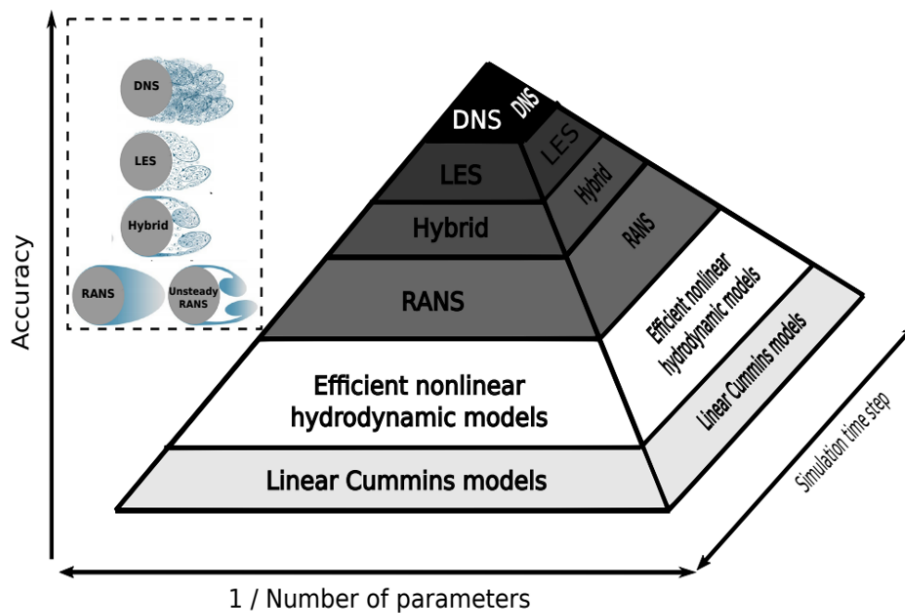
356

### 357 2.2.3 Turbulence modelling

358 WSI can be accompanied by significant turbulent behaviours that dissipate the kinetic energy  
359 and change the fluid behaviours and structural loads. Direct Numerical Simulation (DNS) can  
360 accurately replicate turbulent flows, but this requires solving the Navier-Stokes equations with

361 an extremely high mesh density that most computing facilities can unlikely afford. As a result,  
 362 assumption-based modelling is commonly required. Such assumptions have categorised  
 363 turbulence modelling strategies into several groups, known as Reynolds-Average Navier-  
 364 Stokes equations (RANS), Large-Eddy Simulation (LES) and their combination (Hybrid).  
 365 These methods apply certain numerical treatments to account for the turbulent effects in the  
 366 simulation, allowing savings in cell amount. More details of different turbulence modelling  
 367 approaches can be seen in [69]. Figure 7 illustrates the approaches' levels of fidelity and the  
 368 computational demand.

369



370

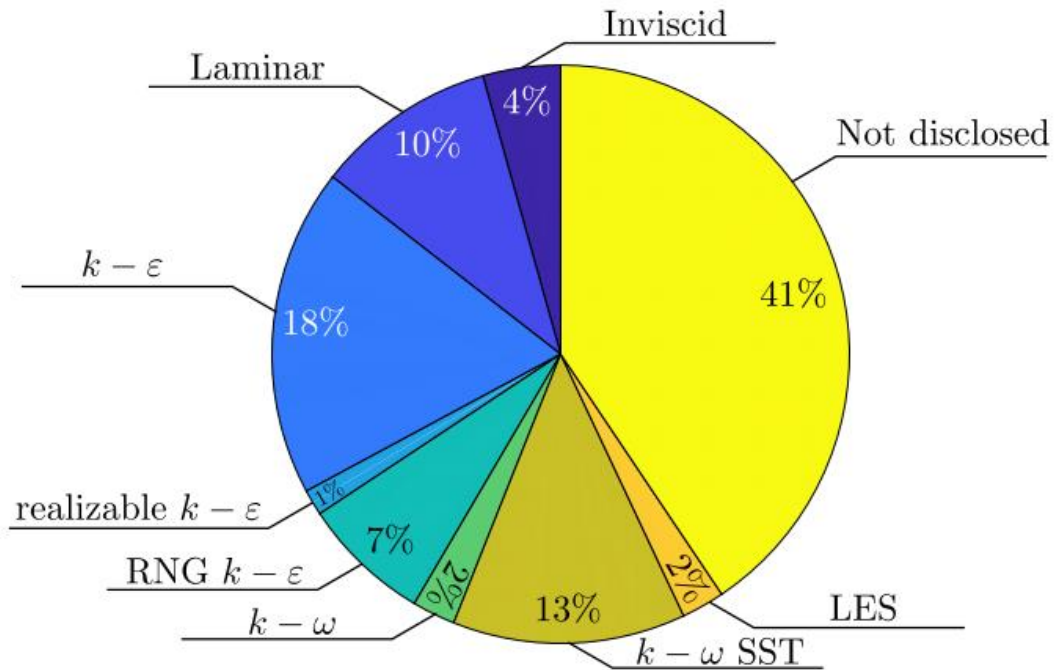
371 Figure 7: Illustration of the fidelity and computational requirement for different turbulence  
 372 modelling methods [70].

373

374 In general, most of the studies of WSI have employed a two-equation model, e.g. the  $k-\omega$  or  $k-$   
 375  $\varepsilon$  model (where  $k$  is the turbulence kinetic energy,  $\omega$  is the specific dissipation rate and  $\varepsilon$  is the  
 376 dissipation rate of turbulence) to close the RANS equations for the turbulent flow [71]. This  
 377 can be corroborated by Windt et al. [72] on the modelling of WEC (Figure 8). Besides two-  
 378 equation models, there are also other RANS-based turbulence models, e.g. Algebraic models,  
 379 one-equation models, Reynolds stress models (RSM). There are two main reasons for RANS-  
 380 based two-equation models to be the mainstream choice: (a) the computational resources  
 381 required for RANS-based two-equation models are much lower than Hybrid or LES, which  
 382 makes RANS simulations mostly affordable by contemporary computing facilities. (b) RANS-  
 383 based two-equation models are seen to provide sufficient accuracy for many 3D WSI

384 applications, so there is normally no necessity to apply a higher-order turbulence modelling  
 385 approach. Validation examples of RANS-based turbulence modelling in various WSI  
 386 applications will be presented in Section 3.

387



388

389 Figure 8: Turbulence models used for CFD modelling of wave energy converters [72].

390

391 Two-equation turbulence models have also been widely used in the past two decades for  
 392 simulating surf zone breaking waves. However, seemingly all the simulations with two-  
 393 equation models (both  $k-\omega$  and  $k-\epsilon$  types) have shown a tendency to overestimate turbulence  
 394 levels for breaking waves, both in the pre- and post-breaking regions. For example, the results  
 395 presented in Brown et al. [75] performed with OpenFOAM using different turbulence models  
 396 have shown over-production of turbulence even in the pre-breaking regions (in this region, the  
 397 waves can be modelled with potential-flow theory and the turbulence is nearly zero). The same  
 398 phenomenon has also been observed in the simulations by Devolder et al. [76] who added  
 399 buoyancy production terms to the  $k-\omega$  branches to eliminate turbulence pollution from the air  
 400 to the water phase.

401 Recently, Larsen and Fuhrman [77] have proved that this problem is due to the unconditional  
 402 instability of two-equation turbulence closure models (both  $k-\omega$  and  $k-\epsilon$  types) in the potential  
 403 flow core region beneath surface waves. A method for formally stabilising two-equation models  
 404 was derived in their work, and it was shown that stabilised two-equation models lead to



405 pronounced improvement in the predicted turbulence and undertow velocity profiles prior to  
406 breaking and in the outer surf zone. Fuhrman and Li [74] analysed a more complicated but  
407 popular turbulence model – the realizable  $k-\varepsilon$  model. They found that this model is conditionally  
408 unstable in the potential flow region beneath surface waves. They likewise stabilized the  
409 realizable  $k-\varepsilon$  model so that the initial conditions would not affect the stability (without  
410 exponential growth of turbulence beneath waves in the potential flow region). However, even  
411 the stabilized two-equation models in Larsen and Fuhrman [77] and Fuhrman and Li [74] were  
412 still rather inaccurate in the inner surf zone (i.e. closer to the shoreline), thus seemingly  
413 requiring yet more advanced methods of achieving turbulence closure.

414 Li et al. [43] analysed more advanced RANS-based Reynolds stress turbulence models (RSMs)  
415 which solve all components of the Reynolds stress and break free from the Boussinesq  
416 approximation (which is a basis for all RANS-based two-equation models). The RSMs were  
417 proved to be reasonable for simulating non-breaking progressive wave trains without having  
418 the problem of over-production of turbulence in the potential flow region beneath surface waves.  
419 The RSM model has also achieved good accuracy in the prediction of coastal breaking waves  
420 on a sloping beach, especially the undertow velocity, as presented in the work of Li et al. [43,73].  
421 The model has also been applied to simulate the deep-water wave instabilities involving wave  
422 breaking, as presented in Li and Fuhrman [44]. The RSM model in terms of the stress- $\omega$  model  
423 is publicly shared through Li [78].

424 Nonetheless, some WSI studies performed with the laminar model (assuming no turbulence  
425 effect) have also shown good accuracy, e.g. [79]. This is probably due to the fact that the waves  
426 are non-breaking and the inertial effect in the problem is stronger than the viscous effect.  
427 Therefore, whether turbulence modelling is required for solving a WSI problem depends on the  
428 physics of the fluid flow in the particular case. For example, Li et al. [79] examined the  
429 Keulegan-Carpenter (KC) number for their study case on wave interaction with a gravity-based  
430 foundation. They found that the turbulence effect is negligible as the KC number is relatively  
431 low, in which case a turbulence modelling approach may not be used.

432

#### 433 2.2.4 Air entrainment

434 Air entrainment can be driven by turbulent motion near the free surface e.g. high-velocity open  
435 channel flows. High-fidelity studies such as DNS have been conducted on air entrainment in  
436 relatively small-scale problems such as in the case of a stationary turbulent hydraulic jump [80].  
437 For larger-scale problems such as spillways, DNS is less practical due to the vast computational  
438 cost. Rather, RANS turbulence models have been widely applied. For example, Lopes et al.  
439 [81] implemented the entrained air flux estimator of Ma et al. [82] in *interFoam*, coupled with

440 the  $k-\omega$  SST turbulence model to simulate the stepped spillway.

441 Air entrainment is also commonly considered in breaking waves. Tomaselli [83] numerically  
442 investigated the air entrainment in breaking waves and their interaction with a monopole also  
443 using *interFoam*, combined with an LES turbulence approach. The air phases in the  
444 aforementioned studies were considered incompressible. Air compressibility has also been  
445 considered and implemented in OpenFOAM as *compressibleInterFoam*. Relevant studies can  
446 be found such as Ferrer et al. [26] and López et al. [28] who studied dam break, plunging wave  
447 impact at a vertical wall, and an oscillating water column.

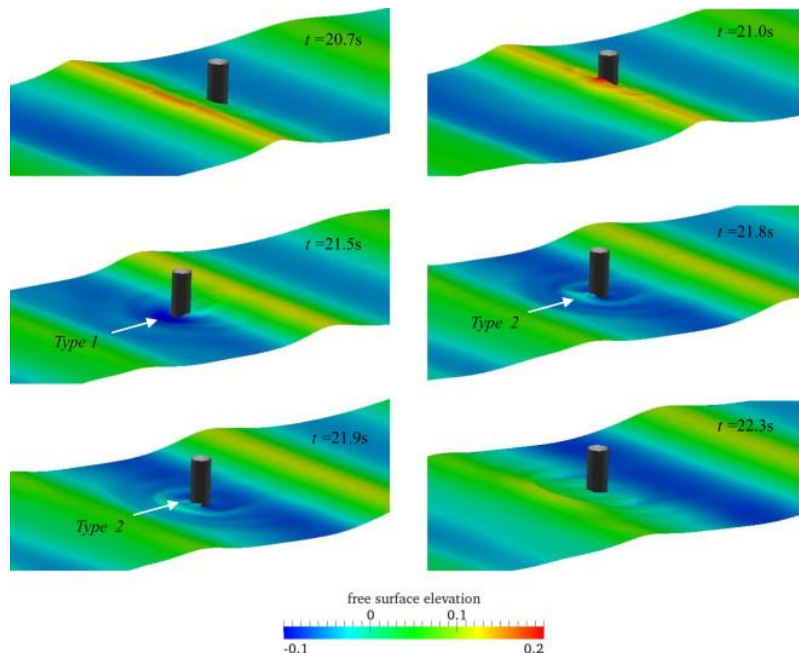
448

### 449 3. WSI modelling

#### 450 3.1 Wave interaction with rigid fixed structures

451 Wave interactions with rigid fixed structures are commonly seen in coastal defence and  
452 offshore wind turbines. Figure 9 provides an example of this type of WSI. As the structure is  
453 fixed, the modelling is relatively simple, as the fixed structure can be treated as a wall boundary  
454 condition that does not involve any structural solutions or dynamic mesh treatment. Therefore,  
455 successful modelling for this type of WSI mainly relies on accurate representation of the fluid  
456 behaviours, i.e. the wave or turbulence modelling, which has been introduced in Section 2.

457



458

459 Figure 9: Uni-directional waves interacting with a fixed cylinder [41]

460 Extensive studies have used OpenFOAM to assess coastal and offshore engineering problems

461 with a fixed structure. Since a sea wall or a breakwater normally expands extensively in the  
462 profile direction, 2D simulations have been widely used to perform analyses and agree well  
463 with wave flume experiments. For example, Morgan and Zan [84] demonstrated OpenFOAM's  
464 ability to produce accurate results for a wide variety of 2D wave conditions and geometries.  
465 They considered submerged breakwater cases where it was found that the numerical predictions  
466 agree with the experimental data, in terms of waveforms and wave amplitude spectra. Their  
467 setup can be used to investigate the dependence of the wave transmission and reflection  
468 properties of the breakwater. Chen et al. [85] performed 2D simulations to predict wave  
469 overtopping on a dike structure. Their prediction of overtopping water level agrees with the  
470 experimental measurements in the time domain. However, the accuracy is based on a stabilised  
471  $k-\omega$  model developed by Larsen and Fuhrman [77], which is essential for accurately modelling  
472 wave propagation in the coastal region and breaking on a structure.

473 In order to account for 3D structures in uni-directional waves but avoid the computational cost  
474 of modelling a whole computational domain in 3D, a 2D-3D coupling model was developed by  
475 Di Paolo et al. [86,87], where 2D was used to solve wave generation from the inlet, stable  
476 propagation towards the structure, and absorption near the outlet; 3D was used only around the  
477 structure. Both one-way and two-way approaches are available. Validation against  
478 experimental data demonstrated that this approach can provide accurate predictions when  
479 considering uni-directional wave conditions.

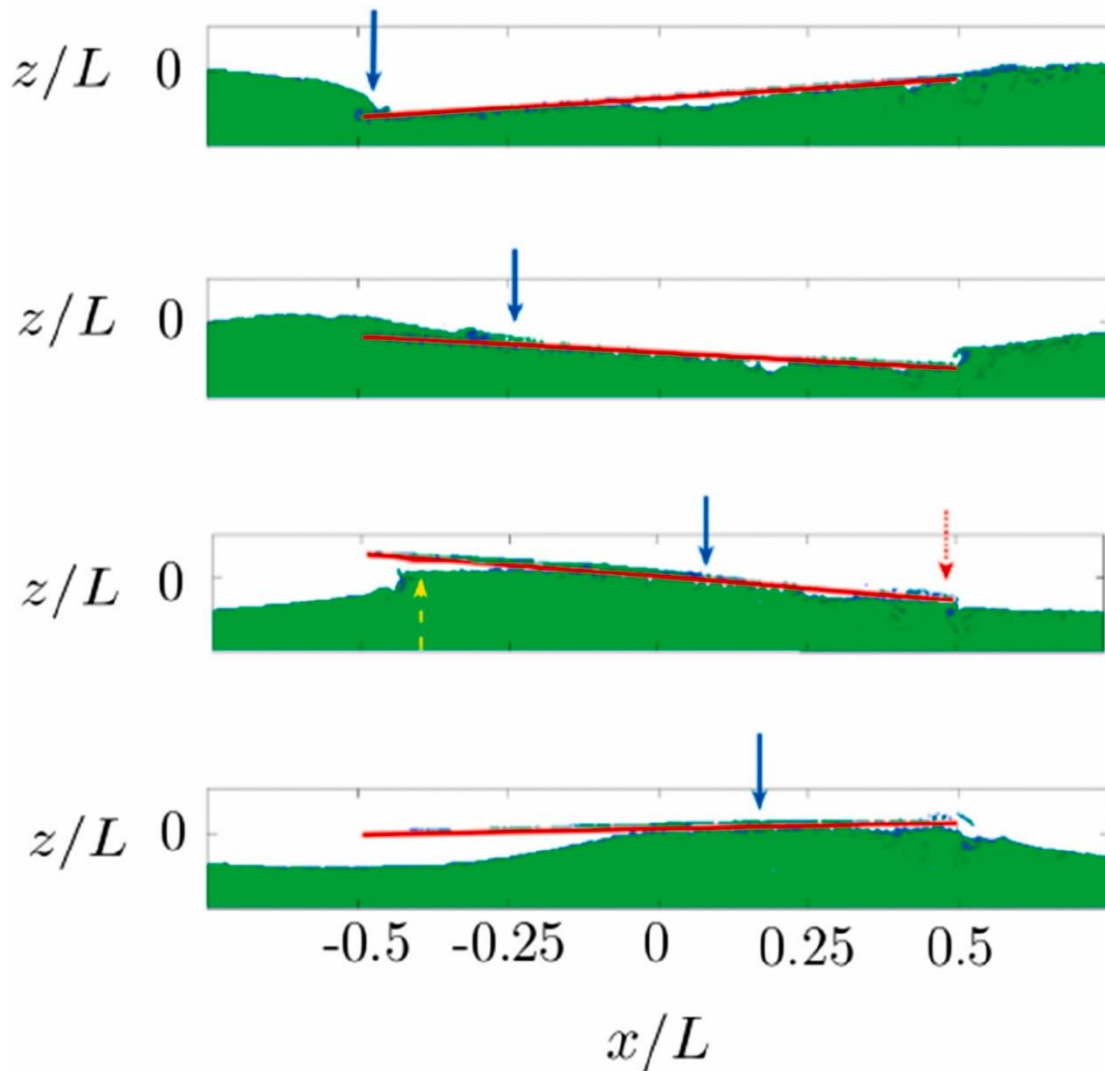
480 Full 3D simulations are required for the 3D multi-directional wave conditions as in real sea  
481 states. However, the wave modelling may be simplified by the spectral approach, which  
482 provides boundary conditions for a small CFD computational domain near the structure. An  
483 example of this treatment is HOS-NWT [88], which has been validated against experiments  
484 [89]. Decorte et al. [90] used the HOS-NWT approach to assess the wave load on a fixed wind  
485 turbine, according to the statistics in non-Gaussian seas.

486

### 487 **3.2 Wave interaction with rigid floating structures**

488 The interaction of waves with a rigid floating body is a two-way process. Waves can induce  
489 body motions, and meanwhile those motions change the surrounding wave field. An example  
490 is shown in Figure 10. To model this type of problem, one of the multiphase solvers of  
491 OpenFOAM is needed to be used, e.g. *interFoam*. However, as the floating body is moving,  
492 simulations need to be carried out with dynamic mesh. The particular module for dynamic mesh  
493 can be *sixDoFRigidBodyMotion*. This module enables us to model the six degrees of freedom  
494 motion under the action of fluid and body forces. The motions in different directions can be  
495 restrained. In summary, *sixDoFRigidBodyMotion* is used for wave-induced motions. In another

496 scenario where the body motion is prescribed rather than induced, another module called  
 497 *solidBody* may be used. *solidBody* allows to model either prescribed linear or angular harmonic  
 498 motions. Such motions might help to model the radiation problem from the prescribed motions  
 499 of a floating object. Simulating prescribed harmonic motions can also help measure the  
 500 hydrodynamic coefficients of a floating object.



501  
 502 Figure 10: Wave interaction with a rigid floating plate [91]

503

504 The main challenge in modelling the dynamic motion of an object is the way the mesh motion  
 505 is handled. Two different methods can be used for six-degree-of-freedom simulations:  
 506 *dynamicMotionSolverFvMesh* and *dynamicOversetFvMesh*, known as the morphing-mesh  
 507 method and the overset method.

508 *dynamicMotionSolverFvMesh* morphs the mesh over every time step, where there are different  
 509 libraries for single-body, *sixdofrigidbodymotion*, and for multi-body, *rigidbodymotion*. The

510 number of cells in the meshing methodology is not changed over time, but the cells might get  
511 distorted or flexed under the action of the motion of the solid body. An inner and an outer  
512 distance around the body are identified. The changes in the cells occur in the area located in  
513 between these two distances. When the motion of the solid body moving under the action of  
514 forces is relatively large, simulations might crash. This commonly happens due to large  
515 distortion of the cells, which needs to be treated by additional steps, such as reconfiguring the  
516 mesh after a certain simulation duration, sliding the mesh, or adding a dedicated motion  
517 interpolating scheme [40,92,93].

518 Extensive work has been carried out by using the morphing technique. In Palm et al. [94], CFD  
519 simulations were performed to model the dynamic response of an ocean WEC exposed to other  
520 waves. In Islam et al. [95], CFD simulations were run to numerically replicate the wave-induced  
521 motion of a floating barge exposed to water waves. More examples of the morphing-mesh  
522 technique in WSI can be found in [59,96–98].

523 *dynamicOversetFvMesh*, known as the overset approach, divides the computational mesh into  
524 two parts: background mesh and overset mesh (where multiple overset regions are possible).  
525 The background mesh denotes the fluid domain which is a fixed Eulerian framework; while the  
526 overset mesh attaches to the structure, moving together with the structure based on its  
527 Lagrangian framework. In this way, both parts of the mesh are not distorted. This method is  
528 particularly used for cases with large motions to overcome the limitations of the  
529 *dynamicMotionSolverFvMesh* for those cases, such as a swinging WEC, large structural  
530 motions induced by rogue waves, planning hulls, or a water-entry process [45,99,100]. At the  
531 present stage, the *overInterDyMFoam* solver is used for overset simulations. The application  
532 of the *overset* method for wave-structure interaction problems is well documented in [101]. The  
533 main challenge of overset, however, is inaccuracies resulting from the interpolation that is  
534 needed to couple the background and overset regions. Due to this, *overset* may violate mass  
535 conservation, and the pressure equation needs to be adjusted implicitly to guarantee the transfer  
536 of fluxes correctly between overlapping regions. Corresponding mitigations may be seen in  
537 [102]. Another potential solution is to build the overset region sufficiently large to avoid  
538 communication locations near the area of interest [100], i.e. farther from the structure, which  
539 might help in predicting the fluid load/impact.

540 Simulations using the overset technique for WSI are also widely conducted. Wu et al. [103]  
541 simulated the dynamic motion of small floating bodies, which may resemble solitary small ice  
542 floes. They used the overset technique to model different geometries of ice floes. They  
543 successfully modelled the wave-induced drift motion of ice floes, having oscillatory motions  
544 in all six degrees of freedom. The model was found to have a great level of accuracy in the

545 prediction of the motion, following validation against experiments. Benites et al. [99] have used  
546 the overset technique to model a WEC rotating with a large angle, and good agreement with  
547 experiments was reported. A power-take-off model is incorporated into the motion solver as a  
548 spring-damping effect. Other overset applications in WSI can be found in [91,104,105].

549

### 550 **3.3 Wave interaction with deformable structures**

551 WSI can also involve a deforming structure. For example, flexible wave energy converters that  
552 deform with waves are shown to have higher efficiency and lower structural risk than rigid ones  
553 [106]; deforming breakwaters demonstrate evidently better wave-attenuation performance than  
554 rigid ones [107]; natural features such as sea ice and vegetations also can deform with waves  
555 [108,109]. To include the deformation significantly increases the computational challenge,  
556 because CFD itself does not contain structural deformation. Therefore, CFD is required to be  
557 coupled with an additional set of computational solid mechanics (CSM) equations to calculate  
558 the structural deformation. If the CSM solution is not fed back to CFD, this mechanism is  
559 known as one-way coupling, and this is commonly applied for stress analyses, where the solid  
560 deformation is inconspicuous while the structural internal stress can be critical, e.g. [110].  
561 However, for WSI processes, deforming structures may also significantly change the  
562 surrounding fluid field, if the structural deformation is large. In order to accurately simulate the  
563 fluid field, the CSM solution is required to be fed back to CFD to enable a two-way Fluid-  
564 Structure Interaction (FSI) process.

565 Waves' interactions with flexible vegetation such as seagrass have also been simulated using  
566 OpenFOAM. Chen et al. [111] presented a coupled wave-vegetation interaction model for  
567 simulating flexible vegetation such as seagrass. The wave hydrodynamics is modelled with  
568 *IHFOam*, and the vegetation motion is solved with the finite element method. The wave and  
569 vegetation models are coupled with an immersed boundary method. The above work used a  
570 combination of solvers, e.g. *interFoam* for CFD and an external solver for CSM, which requires  
571 a third code for coupling, data interpolation and simulation management. This usually results  
572 in the FSI being one-way coupling, thus not fully representing the physics.

573 The realisation of a two-way coupling FSI simulation can be achieved through a partitioned  
574 approach. For every time step of the FSI simulation, (i) the solution of the fluid part is obtained  
575 first, and then the fluid solution is passed as a force on the fluid-solid interface, so that the solid  
576 part can solve the solid deformation. (ii) The deformed solid mesh will also induce the fluid  
577 mesh to deform. In weakly coupled FSI, the solver goes to the next timestep immediately after  
578 step (ii), i.e. without further iterations between fluid and solid domains. This may be acceptable  
579 when the solid deformation is small, as the influence of mesh deformation on the fluid velocity

580 field can be negligible. However, when the solid deformation is large, weakly coupled FSI will  
581 induce errors i.e. inconsistent dynamic and kinematic features between fluid and solid at the  
582 interface, and the errors can be accumulated over each timestep, leading to unreliable results.  
583 To enable a strongly or fully coupled FSI, after step (ii), the fluid solution (i.e. velocity and  
584 pressure of the fluid domain) is updated again in the current timestep, because the fluid domain  
585 has changed with the mesh deformation. If the fluid part is solved again, likewise, the solid  
586 solution will need to be updated again. This can require a large number of iterations until the  
587 fluid and solid parts are fully coupled, i.e. with consistent dynamic and kinematic features at  
588 the interface), while this demonstrates a higher level of accuracy than one-way coupling or  
589 weakly two-way coupling. Such a process that solves fluid and solid separately is therefore  
590 called a partitioned approach. Fluid and solid can also be implicitly solved together, but this  
591 FSI approach is still under development in OpenFOAM, with some early progress shown, such  
592 as [112–114].

593 Based on the partitioned approach, OpenFOAM has made substantial progress in terms of FSI  
594 simulations. Tukovic et al. [115,116] developed an FSI code based on OpenFOAM (*fsiFoam*  
595 solver) with strong two-way coupling as introduced above. An advantage of this OpenFOAM  
596 approach is that it employs the finite-volume method (FVM) for both fluid and solid domains  
597 [115,117]. Most current FSI works involve a combination of solvers, usually with a finite-  
598 volume solver for the fluid flow and a finite-element solver for the structural analysis, e.g. [118],  
599 which requires a third code for coupling, data interpolation and simulation management. Thus,  
600 the combined alternative approaches for the fluid and solid domains will tend to increase  
601 computational costs and imposes limitations on the coupling method. In contrast, the entirely  
602 FVM approach of Tukovic et al. [116] makes an all-in-one solver under the framework of  
603 OpenFOAM.

604 One limitation of *fsiFoam* was that it could only be applied to single-phase fluid modelling.  
605 Therefore, it could not be used for multi-phase applications, e.g. WSI containing both air and  
606 water. In order to simulate hydroelastic problems within OpenFOAM, Huang et al. [119]  
607 incorporated *fsiFoam* with the VOF approach to model multiphase flows, furtherly, with  
608 *waves2foam* to model WSI (named *waveFsiFoam*). In this way, simulations were enabled for  
609 hydroelastic interactions of waves with a large elastic ice sheet [108] and with an elastic  
610 breakwater [107], and the accuracy was validated against experiments. Figure 11 gives an  
611 example of highly-nonlinear breaking waves interacting with a seawall that undertakes large  
612 deformations.

613 In recent years, the development of *fsiFoam* has been combined with a FSI toolbox, *solids4foam*,  
614 led by Cardiff et al. [120]. *solids4foam* has made a significant advancement particularly in

615 structural solutions, by enabling the FSI simulations of viscoelastic, thermoelastic, and  
616 poroelastic solids [120,121]. *solids4foam* is currently deemed to be a long-term FSI framework  
617 of the OpenFOAM family and a robust solver for structural analyses. More applications of  
618 *solids4foam* can be found in [122–124].

619

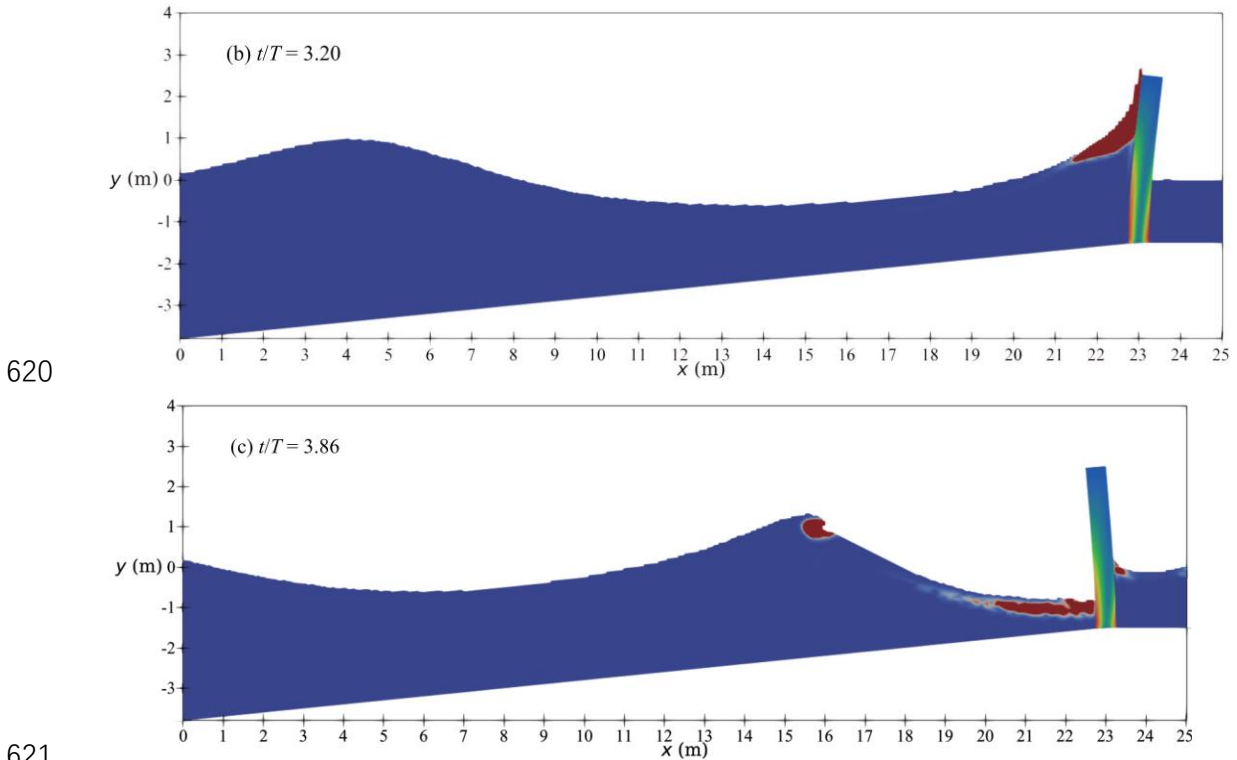


Figure 11: An elastic seawall hit by highly nonlinear breaking waves [125]

623

### 624 3.4 Wave interaction with porous structures

625 The two main methods to model wave interaction with porous structures are the micro- and the  
626 macro-scale approaches. With the micro-scale approach, the detailed geometry of the structure  
627 is resolved explicitly. This allows for high-fidelity investigations of the FSI. Accurate geometry  
628 and fluid flow resolution, however, require a large number of mesh cells, and thus, a high  
629 computational demand. With the macro-scale approach, the effect of the porous structure on  
630 the fluid is applied by means of its bulk effects. Here, the porous structure is not explicitly  
631 resolved but represented by a geometrically defined porous region in which a volume-averaged  
632 macro-scale model is added to the momentum equation through a source term. This approach  
633 cannot reproduce the exact fluid flow inside or close to a porous structure but can provide a  
634 sufficiently accurate replication of the mean flow for many WSI problems. The advantage of  
635 this approach is a smaller computational demand due to the smaller number of mesh cells



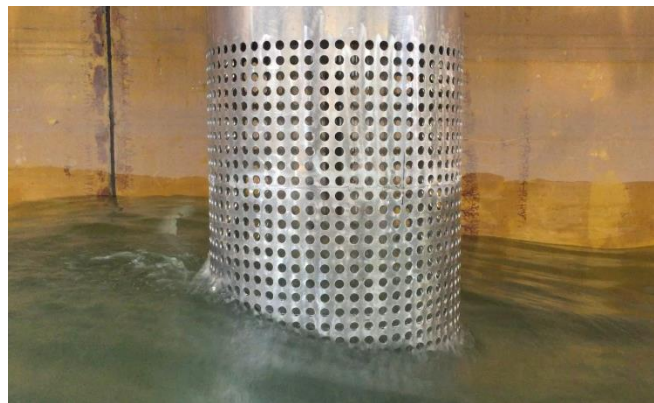
636 required. A comprehensive review on the mathematical foundations and solution techniques of  
637 macro-scale approaches in the context of coastal structures is given in Losada et al. [126].

638 Porous structures can be categorized into large volumetric structures such as breakwaters or  
639 vegetation, and thin porous structures such as perforated or slotted barriers. Depending on the  
640 overall aim of the simulation, either the micro- or the macro-scale approach can be more  
641 suitable. For thin porous structures, the micro-scale approach has been used in most of the  
642 literature, where common objectives are to derive hydrodynamic coefficients, as for instance  
643 by Mentzoni and Kristiansen [127] for an oscillating perforated sheet or by George and Cho  
644 [128] for a sloshing tank with a baffle; or to validate simpler (e.g. analytical) models, as for  
645 example by Poguluri and Cho [129] for a vertically slatted barrier. Conversely, the macro-scale  
646 approach has mainly been applied for thin porous structures when it is challenging to  
647 geometrically resolve the structure or when the overall forces are of interest rather than details  
648 of the flow. Examples are studies on fluid interaction with fish cages by Shim et al. [130] and  
649 Chen and Christensen [131] and with circularly perforated structures by Feichtner et al. [132].  
650 For large volumetric structures, it is common to use a macro-scale approach when the bulk  
651 effects are to be investigated. This avoids challenges in resolving the often complex and  
652 irregular geometries of the structures, and reduces the computational demand significantly  
653 whilst providing sufficiently accurate fluid flow replication. Examples are simulations of wave  
654 interaction with breakwaters by Jensen et al. [133] and Higuera et al. [134,135], or with  
655 vegetation, for instance by Hadadpour et al. [133]. In contrast though, Maza et al. [136]  
656 represented a mangrove forest microscopically by means of a cylinder array and studied  
657 tsunami wave interaction.

658 Within a macro-scale approach, the general formulation of the pressure drop across a porous  
659 structure, commonly called the extended Darcy-Forchheimer law,  $\frac{\Delta p}{x} = au + \frac{b}{2}u|u| + c \frac{\partial u}{\partial x}$ ,  
660 where a, b and c are porosity coefficients that are added to the momentum equation to account  
661 for the effect of the porous structure on the fluid. The linear term represents viscous effects,  
662 dominant for flow regimes with small Re-numbers; the quadratic term represents turbulent  
663 effects with large Re-numbers; the transient term represents effects due to fluid flow  
664 acceleration across the porous voids. The relative importance of the viscous, inertial and  
665 transient terms and the related formulations of the porosity coefficients (a, b, c) are highly  
666 problem-specific and key to accurately representing the properties of the structure and the  
667 corresponding flow regime. For applications to volumetric granular material of coastal  
668 structures, options of formulations are provided in the review by Losada et al. [126]. A  
669 comparison of common formulations for the drag coefficient, b, for slatted barriers can be found  
670 in the work by Poguluri and Cho [129].

671 The porous pressure-drop equation can be implemented in three ways. One option is the  
672 implementation of volumetric porous media with either isotropic or anisotropic characteristics.  
673 This works for both thin and large structures. An additional option for thin structures with  
674 negligible thicknesses, is the porous baffle implementation where a pressure drop is applied  
675 across a surface. An overview of the different types of implementation including illustrations  
676 can be found in Feichtner et al. [137], where the three types have been compared for simulations  
677 of wave interaction with thin perforated sheets and cylinders. The porous baffle or pressure-  
678 jump condition is a standard implementation in OpenFOAM and can be used with *interFoam*  
679 or any other application solver. It introduces the linear and quadratic term of the formulation in  
680 the pressure-drop equation but neglects the transient term, and the input requires the thickness  
681 of the porous structure and the coefficients a and b (in OpenFOAM referred to as D and F for  
682 “Darcy” and “Forchheimer”). A porosity solver for two-phase flow named *porousInterFoam*  
683 was developed but this did not account for the limited amount of fluid inside the porous  
684 structure which can lead to mass conservation problems. This mass conservation issue was  
685 addressed by Jensen et al. [138] and Higuera et al. [134] through implementing macro-scale  
686 porosity based on the volume-averaged RANS (VARANS) equations, in combination with the  
687 wave modelling toolboxes *waves2Foam* [139] (with the *porousWavesFoam* solver by Jensen  
688 et al., [138]) and *OlaFlow/IHFoam* [134,135]. Both use porosity coefficients (a, b, c) based on  
689 granular material by default but it is straightforward to transfer the input to also model thin  
690 porous structures, as in Feichtner et al. [140,137]. Figure 12 provides an example of the macro-  
691 scale simulation approach. The mass conservation issue in porous materials was also addressed  
692 by Romano et al. [141]; their development was combined together with overset and successfully  
693 applied to landslide problems, which could potentially be adaptable to WSI problems.

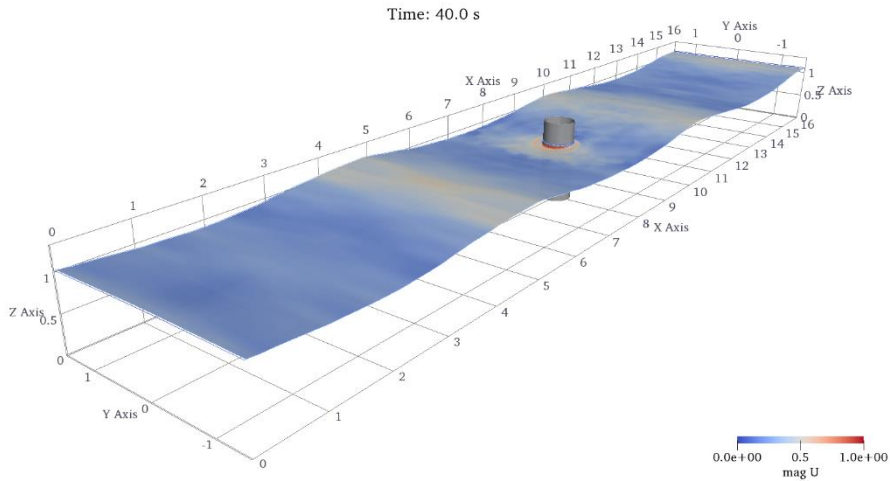
694



695

696

(a) The actual geometry



(b) Simulation

Figure 12: Wave interaction with a porous structure (macro-scale approach) [142]

697

698

699

700

701 A typical benchmark problem for fluid flow across a porous medium but without wave  
 702 interaction is the 2D porous dam-break problem. Also Jensen et al. [138] and Higuera et al.  
 703 [135] have used it for the validation of their porosity solvers where they followed the setups by  
 704 Lin [143] and Liu et al. [144]. Additional examples of CFD modelling for wave interaction  
 705 with microscopically resolved porous structures are works by Wu and Hsiao [145] on solitary  
 706 wave interaction with a submerged slotted barrier, and by Lee et al. [146] on wave interaction  
 707 with a circular perforated caisson breakwater. Further examples of wave interaction with porous  
 708 structures represented by their macro-scale effects are studies by Srineash et al. [147] in the  
 709 context of dams, by Brito et al. [148] on submerged vegetated floodplains and work by Zhao et  
 710 al. [149] on a vertical net panel.

711 In the case of micro-scale porosity modelling, the challenges lie in the accurate representation  
 712 of the geometry of the structure, the correspondingly large number of mesh cells that are  
 713 required and the relatively high computational demand that follows as a consequence. The  
 714 biggest challenge with the macro-scale approach is that the pressure-drop model and the  
 715 formulation of the porosity coefficients (a, b, c) respectively are highly application dependent.  
 716 Since no universal formulation exists, the models rely on coefficients derived from experiments  
 717 or high-fidelity micro-scale models. The solution of a specific engineering problem in the  
 718 context of wave interaction with porous structures generally requires a combination of  
 719 experiments, simpler models, and models with higher fidelity. Another topic, where further  
 720 studies are required, is turbulence modelling for macro-scale porosity representations. Opinions  
 721 differ on whether a model is required at all or whether turbulence effects are already accounted  
 722 for by the pressure-drop formulation. Losada et al. [126] provide a useful overview of the

723 viewpoints and arguments. They also identify future research needing to be done to answer the  
724 unresolved problems.

725 Maza et al. [136] used *IHFoam* to investigate tsunami wave interaction with mangrove forests.  
726 They compared two different conceptual approaches to model the mangrove forests: one is to  
727 directly simulate the detailed geometries of the rigid cylinder array; the other way is to consider  
728 the mangrove forests as a porous rigid media and apply volume-averaging to model the  
729 momentum damping created by the plants. The second approach can be more efficient; however,  
730 it was found that the maximum wave-exerted forces were underestimated.

731

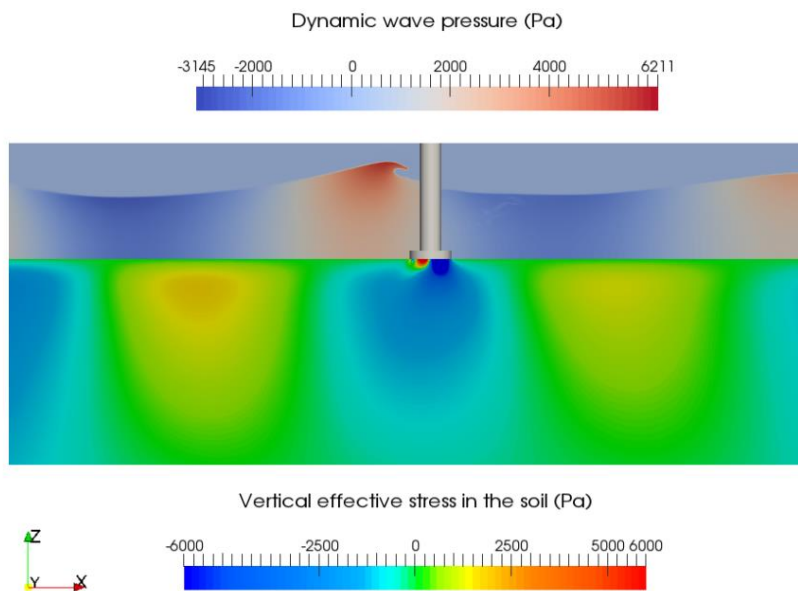
### 732 **3.5 WSI with seabed response**

733 For offshore and coastal structures that are built upon the seabed, the investigation of the  
734 interaction between waves, the structure and the soil is critical for preventing future structure  
735 failures. In conventional geotechnical wave-soil interaction modelling, analytical wave  
736 pressure fields derived from linear or higher-order wave theories are usually applied as an  
737 external force for solving soil responses. However, the analytical solutions are often not  
738 accurate or not applicable to predict the wave-induced seabed responses in the presence of  
739 marine structures. When marine structures with complicated geometries are installed above the  
740 seabed, it will alter the wave field and the forces on the surrounding seabed. In order to achieve  
741 better predictions for wave-structure-seabed interaction problems, multi-physics numerical  
742 models have been developed, where the interaction between nonlinear waves and soil (in the  
743 presence of the structure or not) is modelled. *SedFoam* is a well-known OpenFOAM solver that  
744 includes seabed (or riverbed etc.) as an additional continuum phase, which has shown  
745 prominent performance in the modelling of sediment-transport problems [150].

746 Liu et al. [151] made the first effort to investigate the seabed response in waves using an  
747 integrated CFD approach. They applied a solver in the OpenFOAM framework for two  
748 immiscible incompressible fluids (water and air) to produce a wave field with free surface.  
749 They also implemented a poro-elastic soil solver by discretizing the Biot's equations [152] for  
750 modelling the seabed. Later, Tang and Johannesson [153] extended their work into an  
751 anisotropic model in the quasi-static form in the OpenFOAM framework. The quasi-static  
752 anisotropic poro-elastic solver by Tang and Johannesson [153] was also validated and applied  
753 in the work of Li et al. [79] in which the anisotropic consideration was proven to be practical  
754 for modelling the seabed of medium and coarse sand. Li et al. [154] further developed the soil  
755 model in the partial-dynamic form and incorporated a liquefaction module considering different  
756 liquefaction criteria. The model is opensource at [78], and an example simulation is shown in  
757 Figure 13. Lin et al. [155] used this approach to investigate the nonlinear wave-induced seabed

758 response around mono-pile foundation. Celli et al. [156,157] studied the effect of a submerged  
759 berm on the liquefaction near a rubble mound breakwater in regular and irregular waves. Liang  
760 et al. [158] studied seafloor liquefaction around a pipeline under combined JONSWAP wave  
761 spectrum and current conditions. A variation of the poro-elastic model has been used by Ye et  
762 al. [159] to predict the subsidence of a rubble mound breakwater that exists in real life.

763 Plasticity modelling of the soil in OpenFOAM is also seen in the literature. Tang et al. [121]  
764 implemented an FVM-based code of poro-elasto-plasticity soil model. The model was built  
765 based on the Biot's consolidation theory and combined with a perfect plasticity Mohr-Coulomb  
766 constitutive relation. Elsafti and Oumeraci [160] implemented a multi-yield surface plasticity  
767 model to simulate plastic soil response under cyclic loads in their CFD solver geotechFoam,  
768 also developed in the OpenFOAM framework. A recent work from Shanmugasundaram et al.  
769 [161] has presented a new development to calculate stress fields in seabed, which is capable of  
770 predicting residual-liquefaction problems.



771

772 Figure 13: WSI simulation coupled with the response of seabed (the lower part) [154].

773

774 The soil models for wave-structure-soil interactions have been built based on the constitutive  
775 models developed for onshore geotechnical engineering. Most studies have been performed  
776 based on Biot's [152] consolidation model and its extensions. In fact, the seabed is under  
777 seawater and subjected to complicated environmental loads such as waves, current and seismic  
778 loadings. To date, a generally appropriate seabed constitutive model for marine geotechnical  
779 engineering is not yet available in the public literature. Whether the constitutive relations for  
780 onshore can be applied to offshore remains to be investigated. Meanwhile, most of the existing

781 works have also been limited to an uncoupled approach or semi-coupled approach, rather than  
 782 a fully-coupled approach. As the seabed deformed under strong environmental loading or the  
 783 structure moved its place, it will affect the wave fields and loading distributions in return. Under  
 784 circumstances such as complete liquefaction failures and large deformations, the soil can no  
 785 longer sustain the structure and the structure will move significantly. Therefore, a fully-coupled  
 786 model with strong two-way interaction of the wave-structure-soil system is necessary to be  
 787 developed.

788

#### 789 4. Wave energy converters

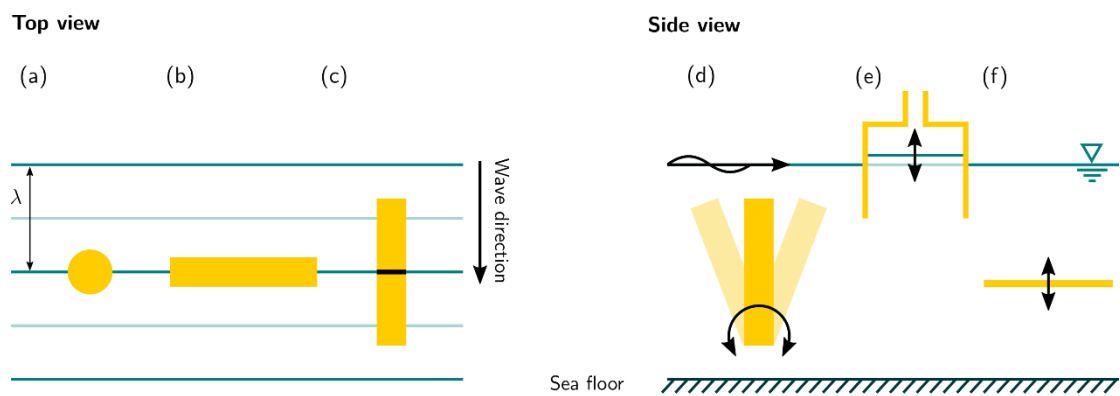
790 In recent years, marine renewable energy systems, such as WECs, supports global efforts to  
 791 adopt clean energies. WECs feature unique characteristics, such as aiming at enhanced body  
 792 motion to extract maximum energy. The large wave conditions and system dynamics of WECs  
 793 involve significant hydrodynamic non-linear effects, which means linear or weakly non-linear  
 794 potential flow methods are not suitable. Therefore, OpenFOAM WSI developments are  
 795 particularly valuable for the modelling of WECs.

796

#### 797 4.1 WEC types

798 Different devices have been envisaged to exploit and harness the wave energy resource. Figure  
 799 14 shows some of the most prominent [162]. Based on different modelling approaches, the  
 800 following section will divide WECs into four categories, i.e. point absorbers, oscillating wave  
 801 surge converters (OWSCs), oscillating water columns (OWCs), and flexible WECs. For a  
 802 specific review of various aspects of WEC modelling in CFD, the interested reader is referred  
 803 to [21].

804



805

Figure 14: Schematic of different WEC types: (a) Point absorber; (b) Terminator; (c) Attenuator; (d) OWSC; (e) OWC; (f) Pressure differential [21].

#### 806 4.1.1 Point absorbers

807 Point absorbers (PAs, Figure 14(a)) are characterised by their small size relative to the incident  
808 wavelength. The large device motion due to the action of energy maximising control systems  
809 [163] challenges the dynamic mesh motion methods [164]. Numerous studies can be found  
810 analysing PAs in the OpenFOAM framework. Studies are conducted in order to, e.g., validate  
811 numerical models [165,19,20], evaluate viscous drag effects [166,167], analyse the device  
812 performance [168], investigate device scaling [169], assess WEC control performance [59], or  
813 for conceptual device design [170].

814

#### 815 4.1.2 Oscillating water columns

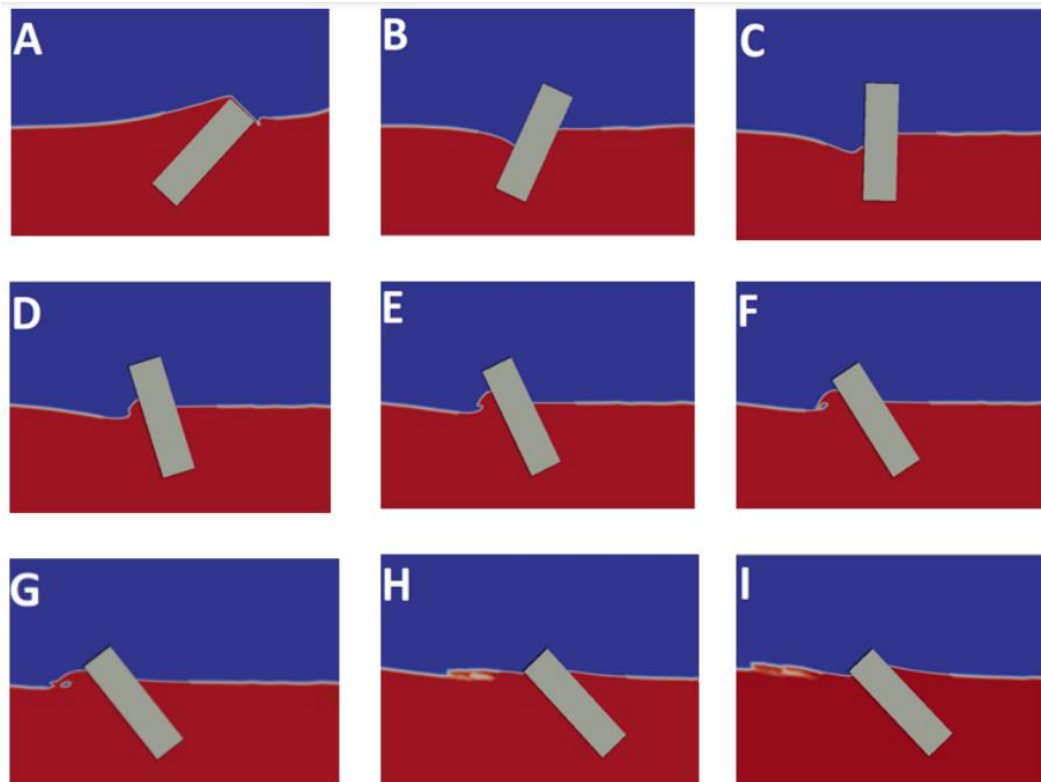
816 Within OWCs (Figure 14(e)), the oscillating water inside a chamber forces entrapped air to  
817 rotate a turbine. When modelling these devices in a CFD framework both highly non-linear free  
818 surface deformations within the air chamber (i.e. sloshing) [171] and air compressibility [27]  
819 may need to be considered. Furthermore, the implementation of the PTO system is of relevance,  
820 which can be achieved, e.g., by modelling a narrow orifice [53,172,173] or implementing a  
821 porous material in a specific zone of the domain [174,175] to model the pressure drop over the  
822 turbine of the real system. CFD models can then be used for performance assessment [176] or  
823 geometry optimisation studies [177,178].

824

#### 825 4.1.3 Oscillating wave surge converters

826 OWSCs (Figure 14(d)) rotate around a hinge point, extracting power from the surging wave  
827 motion. While point absorbers are often characterised by multiple operational DoFs, OWSCs  
828 feature large excursions in a single Degree of Freedom, pitch. For the modelling of these  
829 devices in the OpenFOAM framework, special treatment of the body motion is required, e.g.  
830 by using arbitrary mesh interfaces [92,179,180] An example of the use of mesh morphing  
831 during the analysis of an OWSC can be found in [181]. Figure 15 shows Benites-Munoz et al.'s  
832 work modelling the large rotation of an OWSC using the *overInterDymFoam* [99].

833



834

835

Figure 15: Wave interaction with an oscillating wave energy converter [99]

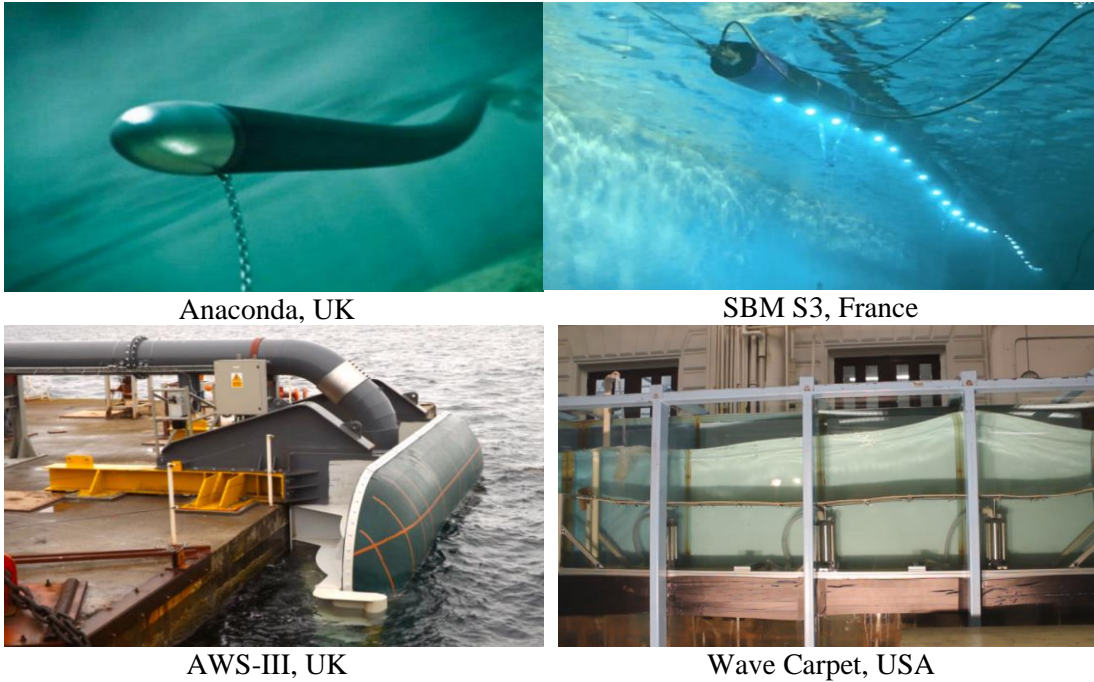
836

#### 837 4.1.4 Flexible WECs

838 The above rigid types of WECs have suffered from structural problems induced by large wave  
 839 loads and insufficient energy output [182]. One potential solution can be applying flexible  
 840 materials for WECs, since the flexibility can effectively mitigate wave loads and the wave-  
 841 induced deformation can be utilised to generate significant power [182]. Some examples of  
 842 flexible WEC devices are shown in Figure 16. The functionality of flexible WECs involves  
 843 complex structural deformations that are based on fully-coupled FSI, i.e., any deformation of  
 844 the structure triggers a response of the wave flow and vice versa; in the WEC field, a modelling  
 845 method with such capability has not been seen in literature, which is pointed out as a crucial  
 846 gap by the recent review of Collins et al. [183]. Fully-coupled FSI can be achieved through  
 847 CFD+CSM, as introduced in Section 3.3. *Solids4foam* may be a good platform to develop  
 848 models for flexible WECs; this is demonstrated through a recent work of Huang et al. using  
 849 fully-coupled CFD+CSM to simulate a “strip shape” WEC [184]. Figure 17 shows the solver’s  
 850 capability of coupling the wave flow and the WEC deformation.

851





Anaconda, UK

SBM S3, France

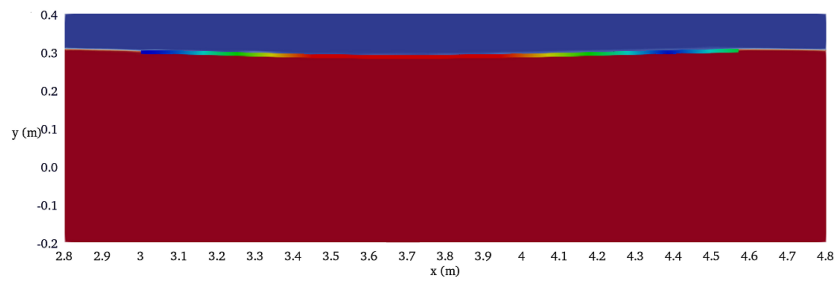
AWS-III, UK

Wave Carpet, USA

852

Figure 16: Flexible WECs: commercial examples

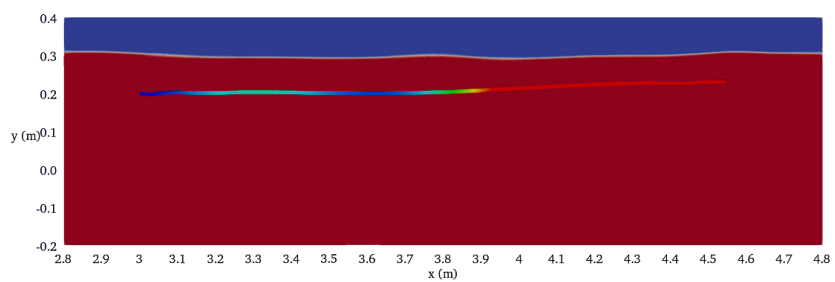
853



854

(b) Simulation: floating case

855



856

(c) Simulation: submerged case

857

Figure 17: Wave interaction with a deformable wave energy converter [184].

858

859

## 860 4.2 Sub-system modelling

861 In addition to the (floating) structure of a WEC, other sub-system components are relevant,

862 when analysing WECs and, thus, should ideally be included in the hydrodynamic modelling  
863 framework. The most prominent sub-systems are the PTO system (often in conjunction with  
864 the energy maximising control system) and the mooring system. When including these sub-  
865 systems within the CFD-based NWT, high-fidelity models are desirable, to avoid spoiling the  
866 underlying fidelity of the (costly) hydrodynamic model.

867

#### 868 4.2.1 Power take-off and control modelling

869 Including a PTO system within the NWT is inherently required in order to assess the power  
870 output of a device. Hence, PTO systems have historically been the first sub-systems to be  
871 included within NWTs. As stated in Section 4.1.3, when modelling OWCs, the PTO can simply  
872 be mimicked by incorporating a narrow orifice or porous media. For PAs (or OWSCs) a simple  
873 implementation of a PTO can be realised by means of a linear spring-damper system, examples  
874 of which can be found in, e.g. [105,179,185]. Non-linear PTO representation (with or without  
875 the inclusion of energy maximising control systems) is more challenging in terms of their  
876 implementation. Coulomb type dampers are implemented in [17,76]. Penalba et al. [186]  
877 present the coupling between an OpenFOAM-based NWT with a fully-nonlinear PTO model,  
878 running in MATLAB.

879

#### 880 4.2.2 Mooring modelling

881 More recently, the inclusion of mooring systems within NWTs is attracting increased attention.  
882 As for the PTO models, different mooring models, with different levels of fidelity and different  
883 levels of associated computational cost, are available. A relatively simple implementation of a  
884 mooring system can be realised through linear springs, i.e. by simply adding a force that is  
885 proportional to the structure displacement [19,20]. For more sophisticated, non-linear mooring  
886 models, coupling of the NWT to external toolboxes is commonly used, examples of which can  
887 be found in [94,187]. Available mooring toolboxes for OpenFOAM include *MooDy* [188] and  
888 *MoorDyn* [189]. Chen and Hall [190] compared these two toolboxes and found their accuracies  
889 are very similar. However, *MooDy* applies a finite-element approach that is slower than  
890 *MoorDyn*, which applies a lumped mass approach. Apart from considering the structural  
891 response in waves, *MooDy* also provides the capability to assess the snap loads in mooring  
892 cables, important for the robustness of mooring systems themselves [191]. Barajas et al. [192]  
893 presented a study using *MooDy* and overset to simulate the motions of a WEC design (without  
894 PTO).

895

896 **5. Conclusions**

897 The present paper has reviewed the progress of various WSI modelling approaches in  
 898 OpenFOAM. The numerical modelling of ocean surface waves and their interactions with fixed,  
 899 floating, deformable or porous structures have been described in detail. Various available  
 900 modelling approaches are suggested, and their pros/cons are discussed. The main conclusions  
 901 of the review are recounted below in Table 1.

902

903 Table 1: Summary on the progress of contemporary WSI developments in OpenFOAM

<b>Topic</b>	<b>Key points</b>
Wave generation and absorption	The relaxation method shows overall stable performance, but it causes additional computational costs. The static boundary method is relatively computationally cheap, but its wave absorption function is complicated and undesirable wave reflection may remain.
Turbulence modelling	Laminar and RANS are suitable for most WSI problems, while cases involving breaking waves are turbulence-demanding. Recent advances have been made in the turbulence modelling of breaking waves with RANS turbulence models.
WSI with rigid bodies.	This is relatively mature. A recommendation is to couple with low-order wave modelling approaches to save computational costs and include real sea states. Most existing studies have considered regular waves – more research works on irregular waves are desired in the future.
WSI with deformable bodies	Two-way fully coupling has been achieved, while the computation can become slow due to FSI iterations. Speeding up computation is a key future development in this field.
WSI with porous structures	Fully resolving the porous structure is computationally prohibitive. Using an empirical approach to mimic porous layers is acceptable but highly depends on the accurate selection of empirical values.
WSI with seabed	The one-way coupling has been relatively mature, but the two-way coupling is lacking.
WECs	PTO is currently incorporated in simulations using oversimplified ways, although it is complicated in real WEC systems.

904

905 This paper is the first review of WSI modelling for OpenFOAM that has covered such  
906 comprehensive topics. To the best knowledge of the authors, this is also currently the widest  
907 WSI review in the entire CFD community. This contribution is expected to help readers better  
908 understand the relevant CFD methodologies and provide directions on the selection of models  
909 as well as the future development of the field.

910

## 911 **References**

- 912 [1] A.E. Heins, Water waves over a channel of finite depth with a submerged plane barrier,  
913 *Canadian Journal of Mathematics*. 2 (1950) 210–222.
- 914 [2] J.R. Morison, J.W. Johnson, S.A. Schaaf, The force exerted by surface waves on piles,  
915 *Journal of Petroleum Technology*. 2 (1950) 149–154.
- 916 [3] J.B. Keller, F.C. Karal Jr, Surface wave excitation and propagation, *Journal of Applied*  
917 *Physics*. 31 (1960) 1039–1046.
- 918 [4] R.C.T. Rainey, A new equation for calculating wave loads on offshore structures, *Journal*  
919 *of Fluid Mechanics*. 204 (1989) 295–324.
- 920 [5] O.M. Faltinsen, J.N. Newman, T. Vinje, Nonlinear wave loads on a slender vertical  
921 cylinder, *Journal of Fluid Mechanics*. 289 (1995) 179–198.
- 922 [6] B.Z. Zhou, G.X. Wu, Resonance of a tension leg platform excited by third-harmonic force  
923 in nonlinear regular waves, *Philosophical Transactions of the Royal Society A:*  
924 *Mathematical, Physical and Engineering Sciences*. 373 (2015) 20140105.
- 925 [7] B.Z. Zhou, G.X. Wu, B. Teng, Fully nonlinear wave interaction with freely floating non-  
926 wall-sided structures, *Engineering Analysis with Boundary Elements*. 50 (2015) 117–132.
- 927 [8] Y. Sun, G. Xi, Z. Sun, A fully Lagrangian method for fluid–structure interaction problems  
928 with deformable floating structure, *Journal of Fluids and Structures*. 90 (2019) 379–395.
- 929 [9] M.S. Shadloo, G. Oger, D. Le Touzé, Smoothed particle hydrodynamics method for fluid  
930 flows, towards industrial applications: Motivations, current state, and challenges,  
931 *Computers & Fluids*. 136 (2016) 11–34.
- 932 [10] P. Higuera, olaFlow: CFD for waves [Software]., (2017).  
933 <https://doi.org/10.5281/zenodo.1297013>.
- 934 [11] H. Bihs, W. Wang, C. Pakozdi, A. Kamath, REEF3D:: FNNP—A flexible fully nonlinear  
935 potential flow solver, *Journal of Offshore Mechanics and Arctic Engineering*. 142 (2020).
- 936 [12] T.R. Keen, T.J. Campbell, J.D. Dykes, P.J. Martin, Gerris Flow Solver: Implementation  
937 and Application, *NAVAL RESEARCH LAB STENNIS DETACHMENT STENNIS*  
938 *SPACE CENTER MS OCEANOGRAPHY DIV*, 2013.
- 939 [13] D.M. Greaves, Viscous waves and wave-structure interaction in a tank using adapting  
940 quadtree grids, *Journal of Fluids and Structures*. 23 (2007) 1149–1167.
- 941 [14] J. Sanders, J.E. Dolbow, P.J. Mucha, T.A. Laursen, A new method for simulating rigid  
942 body motion in incompressible two-phase flow, *International Journal for Numerical*  
943 *Methods in Fluids*. 67 (2011) 713–732.
- 944 [15] J. Westphalen, D.M. Greaves, A. Raby, Z.Z. Hu, D.M. Causon, C.G. Mingham, P.  
945 Omidvar, P.K. Stansby, B.D. Rogers, Investigation of wave-structure interaction using  
946 state of the art CFD techniques, *Open Journal of Fluid Dynamics*. 4 (2014) 18.
- 947 [16] L. Sjökvist, M. Göteman, Peak forces on wave energy linear generators in tsunami and  
948 extreme waves, *Energies*. 10 (2017) 1323.
- 949 [17] L. Sjökvist, J. Wu, E. Ransley, J. Engström, M. Eriksson, M. Göteman, Numerical models  
950 for the motion and forces of point-absorbing wave energy converters in extreme waves,  
951 *Ocean Engineering*. 145 (2017) 1–14. <https://doi.org/10.1016/j.oceaneng.2017.08.061>.
- 952 [18] E. Ransley, S. Yan, S.A. Brown, T. Mai, D. Graham, Q. Ma, P.-H. Musiedlak, A.P.  
953 Engsig-Karup, C. Eskilsson, Q. Li, A blind comparative study of focused wave

- 954 interactions with a fixed FPSO-like structure (CCP-WSI Blind Test Series 1),  
 955 International Journal of Offshore and Polar Engineering. 29 (2019) 113–127.
- 956 [19] E. Ransley, S. Yan, S. Brown, M. Hann, D. Graham, C. Windt, P. Schmitt, J. Davidson,  
 957 J. Ringwood, P.-H. Musiedlak, A blind comparative study of focused wave interactions  
 958 with floating structures (CCP-WSI Blind Test Series 3), International Journal of Offshore  
 959 and Polar Engineering. 30 (2020) 1–10.
- 960 [20] E.J. Ransley, S.A. Brown, M. Hann, D.M. Greaves, C. Windt, J. Ringwood, J. Davidson,  
 961 P. Schmitt, S. Yan, J.X. Wang, J.H. Wang, Q. Ma, Z. Xie, G. Giorgi, J. Hughes, A.  
 962 Williams, I. Masters, Z. Lin, H. Chen, L. Qian, Z. Ma, Q. Chen, H. Ding, J. Zang, J. van  
 963 Rij, Y.-H. Yu, Z. Li, B. Bouscasse, G. Ducrozet, H. Bingham, Focused wave interactions  
 964 with floating structures: a blind comparative study, Proceedings of the Institution of Civil  
 965 Engineers - Engineering and Computational Mechanics. 174 (2021) 46–61.  
 966 <https://doi.org/10.1680/jencm.20.00006>.
- 967 [21] C. Windt, J. Davidson, J.V. Ringwood, High-fidelity numerical modelling of ocean wave  
 968 energy systems: A review of computational fluid dynamics-based numerical wave tanks,  
 969 Renewable and Sustainable Energy Reviews. 93 (2018) 610–630.  
 970 <https://doi.org/10.1016/j.rser.2018.05.020>.
- 971 [22] P. Schmitt, C. Windt, J. Davidson, J.V. Ringwood, T. Whittaker, Beyond VoF: alternative  
 972 OpenFOAM solvers for numerical wave tanks, Journal of Ocean Engineering and Marine  
 973 Energy. 6 (2020) 277–292.
- 974 [23] H. Yang, J. Lu, S. Yan, Preliminary numerical study on oil spilling from a DHT, in: The  
 975 Twenty-Fourth International Ocean and Polar Engineering Conference, OnePetro, 2014.
- 976 [24] F. Gao, Z.H. Ma, J. Zang, D.M. Causon, C.G. Mingham, L. Qian, Simulation of breaking  
 977 wave impact on a vertical wall with a compressible two-phase flow, model, in: The  
 978 Twenty-Fifth International Ocean and Polar Engineering Conference, OnePetro, 2015.
- 979 [25] B.R. Seiffert, R.C. Ertekin, I.N. Robertson, Wave loads on a coastal bridge deck and the  
 980 role of entrapped air, Applied Ocean Research. 53 (2015) 91–106.
- 981 [26] P.M. Ferrer, D.M. Causon, L. Qian, C.G. Mingham, Z.H. Ma, Numerical simulation of  
 982 wave slamming on a flap type oscillating wave energy device, Proceedings of the  
 983 Twentysixth. (2016).
- 984 [27] I. Simonetti, L. Cappiotti, H. Elsafti, H. Oumeraci, Evaluation of air compressibility  
 985 effects on the performance of fixed OWC wave energy converters using CFD modelling,  
 986 Renewable Energy. 119 (2018) 741–753.
- 987 [28] I. López, R. Carballo, F. Taveira-Pinto, G. Iglesias, Sensitivity of OWC performance to  
 988 air compressibility, Renewable Energy. 145 (2020) 1334–1347.
- 989 [29] C. Eskilsson, J. Palm, J.P. Kofoed, E. Friis-Madsen, CFD study of the overtopping  
 990 discharge of the Wave Dragon wave energy converter, Renewable Energies Offshore.  
 991 (2015) 287–294.
- 992 [30] J. Roenby, H. Bredmose, H. Jasak, A computational method for sharp interface advection,  
 993 Royal Society Open Science. 3 (2016) 160405.
- 994 [31] S.S. Deshpande, L. Anumolu, M.F. Trujillo, Evaluating the performance of the two-phase  
 995 flow solver interFoam, Computational Science & Discovery. 5 (2012) 014016.
- 996 [32] B.E. Larsen, D.R. Fuhrman, J. Roenby, Performance of interFoam on the simulation of  
 997 progressive waves, Coastal Engineering Journal. 61 (2019) 380–400.
- 998 [33] V. Vukčević, J. Roenby, I. Gatin, H. Jasak, A sharp free surface finite volume method  
 999 applied to gravity wave flows, ArXiv Preprint ArXiv:1804.01130. (2018).
- 1000 [34] V. Vukčević, H. Jasak, I. Gatin, Implementation of the ghost fluid method for free surface  
 1001 flows in polyhedral finite volume framework, Computers & Fluids. 153 (2017) 1–19.
- 1002 [35] P. Peltonen, P. Kanninen, E. Laurila, V. Vuorinen, The ghost fluid method for openfoam:  
 1003 A comparative study in marine context, Ocean Engineering. 216 (2020) 108007.
- 1004 [36] CFD Direct, Interface Capturing in OpenFOAM, (2020).  
 1005 <https://cfd.direct/openfoam/free-software/multiphase-interface-capturing/>.
- 1006 [37] J.S. Piña, D. Godino, S. Corzo, D. Ramajo, AIR INJECTION IN VERTICAL WATER  
 1007 COLUMN: EXPERIMENTAL TEST AND NUMERICAL SIMULATION USING

- 1008 VOLUME OF FLUID AND TWO-FLUID METHODS, Chemical Engineering Science.  
 1009 (2022) 117665.
- 1010 [38] A.J.-C. de Saint-Venant, Théorie du mouvement non-permanent des eaux, avec  
 1011 application aux crues des rivières et à l'introduction des marées dans leur lit, CR Acad.  
 1012 Sci. Paris. 73 (1871) 5.
- 1013 [39] Ž. Tuković, H. Jasak, A moving mesh finite volume interface tracking method for surface  
 1014 tension dominated interfacial fluid flow, Computers & Fluids. 55 (2012) 70–84.
- 1015 [40] L. Huang, G. Thomas, Simulation of Wave Interaction With a Circular Ice Floe, Journal  
 1016 of Offshore Mechanics and Arctic Engineering. 141 (2019) 041302.
- 1017 [41] L.F. Chen, J. Zang, A.J. Hillis, G.C.J. Morgan, A.R. Plummer, Numerical investigation  
 1018 of wave–structure interaction using OpenFOAM, Ocean Engineering. 88 (2014) 91–109.
- 1019 [42] ITTC, Seakeeping Experiments, Recommended Procedures and Guidelines. (2017).
- 1020 [43] Y. Li, B. Larsen, D.R. Fuhrman, Reynolds stress turbulence modelling of surf zone  
 1021 breaking waves, Journal of Fluid Mechanics. 937 (2022) A7.
- 1022 [44] Y. Li, D.R. Fuhrman, Computational fluid dynamics simulation of deep-water wave  
 1023 instabilities involving wave breaking, Journal of Offshore Mechanics and Arctic  
 1024 Engineering. (2022) 144.2. [45] S. Lyu, L. Huang, G. Thomas, Motions of a Floating  
 1025 Body Induced by Rogue Waves, The 14th OpenFOAM Workshop. (2019).
- 1026 [46] H. Bredmose, N.G. Jacobsen, Breaking wave impacts on offshore wind turbine  
 1027 foundations: focused wave groups and CFD, in: International Conference on Offshore  
 1028 Mechanics and Arctic Engineering, 2010: pp. 397–404.
- 1029 [47] P. Schmitt, B. Elsaesser, On the use of OpenFOAM to model oscillating wave surge  
 1030 converters, Ocean Engineering. 108 (2015) 98–104.  
 1031 <https://doi.org/10.1016/j.oceaneng.2015.07.055>.
- 1032 [48] P. Higuera, I.J. Losada, J.L. Lara, Three-dimensional numerical wave generation with  
 1033 moving boundaries, Coastal Engineering. 101 (2015) 35–47.
- 1034 [49] P. Schmitt, B. Elsaesser, A Review of Wave Makers for 3D Numerical Simulations, VI  
 1035 International Conference on Computational Methods in Marine Engineering (MARINE  
 1036 2015). (2015) 1–10.
- 1037 [50] C. Windt, J. Davidson, P. Schmitt, J. V Ringwood, Assessment of Numerical Wave  
 1038 Makers, (2017).
- 1039 [51] N.G. Jacobsen, D.R. Fuhrman, J. Fredsøe, A wave generation toolbox for the open-source  
 1040 CFD library: OpenFoam®, International Journal for Numerical Methods in Fluids. 70  
 1041 (2012) 1073–1088. <https://doi.org/10.1002/flid.2726>.
- 1042 [52] Z.Z. Hu, D. Greaves, A. Raby, Numerical wave tank study of extreme waves and wave-  
 1043 structure interaction using OpenFoam®, Ocean Engineering. 126 (2016) 329–342.
- 1044 [53] T. Vyzikas, S. Deshoulières, O. Giroux, M. Barton, D. Greaves, Numerical study of fixed  
 1045 Oscillating Water Column with RANS-type two-phase CFD model, Renewable Energy.  
 1046 102 (2017) 294–305.
- 1047 [54] N. Bruinsma, B.T. Paulsen, N.G. Jacobsen, Validation and application of a fully nonlinear  
 1048 numerical wave tank for simulating floating offshore wind turbines, Ocean Engineering.  
 1049 147 (2018) 647–658.
- 1050 [55] N. Bruinsma, Validation and application of a fully nonlinear numerical wave tank, Master  
 1051 Thesis, TU Delft, 2016.
- 1052 [56] IHCantabria, IHFoam manual, (2014). <https://ihfoam.ihcantabria.com/>.
- 1053 [57] B. Devolder, P. Rauwoens, P. Troch, Application of a buoyancy-modified k-  
 1054  $\omega$  SST turbulence model to simulate wave run-up around a monopile subjected to  
 1055 regular waves using OpenFOAM®, Coastal Engineering. 125 (2017) 81–94.
- 1056 [58] H.G. Guler, C. Baykal, T. Arikawa, A.C. Yalciner, Numerical assessment of tsunami  
 1057 attack on a rubble mound breakwater using OpenFOAM®, Applied Ocean Research. 72  
 1058 (2018) 76–91.
- 1059 [59] C. Windt, N. Faedo, M. Penalba, F. Dias, J.V. Ringwood, Reactive control of wave energy  
 1060 devices—the modelling paradox, Applied Ocean Research. 109 (2021) 102574.
- 1061 [60] P. Higuera, J.L. Lara, I.J. Losada, Realistic wave generation and active wave absorption

- 1062 for Navier-Stokes models. Application to OpenFOAM®, Coastal Engineering. 71 (2013)  
 1063 102–118. <https://doi.org/10.1016/j.coastaleng.2012.07.002>.
- 1064 [61] IHCantabria, IHFOAM Manual 15th July 2014, (2014).
- 1065 [62] H.A. Schäffer, G. Klopman, Review of multidirectional active wave absorption methods,  
 1066 Journal of Waterway, Port, Coastal, and Ocean Engineering. 126 (2000) 88–97.
- 1067 [63] P. Higuera, Enhancing active wave absorption in RANS models, Applied Ocean Research.  
 1068 94 (2020) 102000.
- 1069 [64] M. Borsboom, N.G. Jacobsen, A generating-absorbing boundary condition for dispersive  
 1070 waves, International Journal for Numerical Methods in Fluids. 93 (2021) 2443–2467.
- 1071 [65] C. Windt, J. Davidson, P. Schmitt, J. V. Ringwood, On the Assessment of Numerical  
 1072 Wave Makers in CFD simulations, Journal of Marine Science and Engineering. 7 (2019).  
 1073 <https://doi.org/10.3390/JMSE7020047>.
- 1074 [66] K.O. Connell, A. Cashman, Development of a numerical wave tank with reduced  
 1075 discretization error, in: 2016 International Conference on Electrical, Electronics, and  
 1076 Optimization Techniques (ICEEOT), IEEE, 2016: pp. 3008–3012.
- 1077 [67] P. Schmitt, B. Elsaesser, A review of wave makers for 3D numerical simulations, in:  
 1078 MARINE VI: Proceedings of the VI International Conference on Computational Methods  
 1079 in Marine Engineering, CIMNE, 2015: pp. 437–446.
- 1080 [68] C. Windt, J. Davidson, P. Schmitt, J.V. Ringwood, On the assessment of numerical wave  
 1081 makers in CFD simulations, Journal of Marine Science and Engineering. 7 (2019) 47.
- 1082 [69] B. Pena, L. Huang, A review on the turbulence modelling strategy for ship hydrodynamic  
 1083 simulations, Ocean Engineering. (2021).
- 1084 [70] J. Davidson, R. Costello, Efficient nonlinear hydrodynamic models for wave energy  
 1085 converter design—A scoping study, Journal of Marine Science and Engineering. 8 (2020)  
 1086 35.
- 1087 [71] D. Khojasteh, S. Tavakoli, A. Dashtimanesh, A. Dolatshah, L. Huang, W. Glamore, M.  
 1088 Sadat-Noori, G. Iglesias, Numerical analysis of shipping water impacting a step structure,  
 1089 Ocean Engineering. 209 (2020) 107517.
- 1090 [72] C. Windt, J. Davidson, J.V. Ringwood, Investigation of Turbulence Modeling for Point-  
 1091 Absorber-Type Wave Energy Converters, Energies. 14 (2021) 26.
- 1092 [73] Y. Li, M.B. Fredberg, B.E. Larsen, D.R. Fuhrman, Simulating Breaking Waves with the  
 1093 Reynolds Stress Turbulence Model, Coastal Engineering Proceedings. (2020) 17–17.
- 1094 [74] D.R. Fuhrman, Y. Li, Instability of the realizable  $k-\epsilon$  turbulence model beneath surface  
 1095 waves, Physics of Fluids. 32 (2020) 115108.
- 1096 [75] S.A. Brown, D.M. Greaves, V. Magar, D.C. Conley, Evaluation of turbulence closure  
 1097 models under spilling and plunging breakers in the surf zone, Coastal Engineering. 114  
 1098 (2016) 177–193.
- 1099 [76] B. Devolder, V. Stratigaki, P. Troch, P. Rauwoens, CFD Simulations of Floating Point  
 1100 Absorber Wave Energy Converter Arrays Subjected to Regular Waves, Energies. 11  
 1101 (2018) 641. <https://doi.org/10.3390/en11030641>.
- 1102 [77] B.E. Larsen, D.R. Fuhrman, On the over-production of turbulence beneath surface waves  
 1103 in Reynolds-averaged Navier–Stokes models, Journal of Fluid Mechanics. 853 (2018)  
 1104 419–460.
- 1105 [78] Y. Li, The Reynolds Stress Turbulence Model,  
 1106 <https://github.com/LiYZPearl/ReynoldsStressTurbulenceModels>., 2021.
- 1107 [79] Y. Li, M.C. Ong, T. Tang, Numerical analysis of wave-induced poro-elastic seabed  
 1108 response around a hexagonal gravity-based offshore foundation, Coastal Engineering.  
 1109 136 (2018) 81–95.
- 1110 [80] M. Mortazavi, V. Le Chenadec, P. Moin, A. Mani, Direct numerical simulation of a  
 1111 turbulent hydraulic jump: turbulence statistics and air entrainment, Journal of Fluid  
 1112 Mechanics. 797 (2016) 60–94.
- 1113 [81] P. Lopes, J. Leandro, R.F. Carvalho, Self-aeration modelling using a sub-grid volume-of-  
 1114 fluid model, International Journal of Nonlinear Sciences and Numerical Simulation. 18  
 1115 (2017) 559–574.

- 1116 [82] J. Ma, A.A. Oberai, D.A. Drew, R.T. Lahey Jr, M.C. Hyman, A comprehensive sub-grid  
1117 air entrainment model for RaNS modeling of free-surface bubbly flows, *The Journal of*  
1118 *Computational Multiphase Flows*. 3 (2011) 41–56.
- 1119 [83] P.D. Tomaselli, A methodology for air entrainment in breaking waves and their  
1120 interaction with a mono-pile, PhD Thesis, Technical University of Denmark Lyngby,  
1121 Denmark, 2016.
- 1122 [84] G. Morgan, J. Zang, Application of OpenFOAM to coastal and offshore modelling, *The*  
1123 *26th IWWFEB*. Athens, Greece. (2011).
- 1124 [85] W. Chen, J.J. Warmink, M.R.A. Van Gent, S. Hulscher, Numerical modelling of wave  
1125 overtopping at dikes using OpenFOAM®, *Coastal Engineering*. 166 (2021) 103890.
- 1126 [86] B. Di Paolo, J.L. Lara, G. Barajas, Í.J. Losada, Wave and structure interaction using multi-  
1127 domain couplings for Navier-Stokes solvers in OpenFOAM®. Part I: Implementation and  
1128 validation, *Coastal Engineering*. 164 (2021) 103799.  
1129 <https://doi.org/10.1016/j.coastaleng.2020.103799>.
- 1130 [87] B. Di Paolo, J.L. Lara, G. Barajas, Í.J. Losada, Waves and structure interaction using  
1131 multi-domain couplings for Navier-Stokes solvers in OpenFOAM®. Part II: Validation  
1132 and application to complex cases, *Coastal Engineering*. 164 (2021) 103818.  
1133 <https://doi.org/10.1016/j.coastaleng.2020.103818>.
- 1134 [88] G. Ducrozet, F. Bonnefoy, D. Le Touzé, P. Ferrant, A modified high-order spectral  
1135 method for wavemaker modeling in a numerical wave tank, *European Journal of*  
1136 *Mechanics-B/Fluids*. 34 (2012) 19–34.
- 1137 [89] B. Quinn, Validation of the High Order Spectral (HOS) Method for Extreme and Breaking  
1138 Waves and Coupling of the HOS-Numerical Wave Tank Model with OpenFOAM,  
1139 Master’s Thesis, University of Stavanger, Norway, 2019.
- 1140 [90] G. Decorte, A. Toffoli, G. Lombaert, J. Monbaliu, On the use of a domain decomposition  
1141 strategy in obtaining response statistics in non-Gaussian seas, *Fluids*. 6 (2021) 28.
- 1142 [91] S. Tavakoli, A.V. Babanin, Wave energy attenuation by drifting and non-drifting floating  
1143 rigid plates, *Ocean Engineering*. 226 (2021) 108717.  
1144 <https://doi.org/10.1016/j.oceaneng.2021.108717>.
- 1145 [92] P. Schmitt, B. Elsaesser, On the use of OpenFOAM to model oscillating wave surge  
1146 converters, *Ocean Engineering*. 108 (2015) 98–104.  
1147 <https://doi.org/10.1016/j.oceaneng.2015.07.055>.
- 1148 [93] J. Palm, C. Eskilsson, Facilitating Large-Amplitude Motions of Wave Energy Converters  
1149 in OpenFOAM by a Modified Mesh Morphing Approach, in: *14th European Wave and*  
1150 *Tidal Energy Conference*, European Tidal and Wave Energy Conference, 2021.
- 1151 [94] J. Palm, C. Eskilsson, G.M. Paredes, L. Bergdahl, Coupled mooring analysis for floating  
1152 wave energy converters using CFD: Formulation and validation, *International Journal of*  
1153 *Marine Energy*. 16 (2016) 83–99.
- 1154 [95] H. Islam, S.C. Mohapatra, J. Gadelho, C.G. Soares, OpenFOAM analysis of the wave  
1155 radiation by a box-type floating structure, *Ocean Engineering*. 193 (2019) 106532.
- 1156 [96] M. Yan, X. Ma, W. Bai, Z. Lin, Y. Li, Numerical simulation of wave interaction with  
1157 payloads of different postures using OpenFOAM, *Journal of Marine Science and*  
1158 *Engineering*. 8 (2020) 433.
- 1159 [97] S.C. Mohapatra, H. Islam, C. Guedes Soares, Boussinesq model and CFD simulations of  
1160 non-linear wave diffraction by a floating vertical cylinder, *Journal of Marine Science and*  
1161 *Engineering*. 8 (2020) 575.
- 1162 [98] M. Yousefifard, A. Graylee, A numerical solution of the wave–body interactions for a  
1163 freely floating vertical cylinder in different water depths using OpenFOAM, *Journal of*  
1164 *the Brazilian Society of Mechanical Sciences and Engineering*. 43 (2021) 1–14.
- 1165 [99] D. Benites-Munoz, L. Huang, E. Anderlini, J.R. Marín-Lopez, G. Thomas,  
1166 Hydrodynamic Modelling of An Oscillating Wave Surge Converter Including Power  
1167 Take-Off, *Journal of Marine Science and Engineering*. 8 (2020) 771.
- 1168 [100] L. Huang, S. Tavakoli, M. Li, A. Dolatshah, B. Pena, B. Ding, A. Dashtimanesh, CFD  
1169 analyses on the water entry process of a freefall lifeboat, *Ocean Engineering*. 232 (2021)



1170 109115.

1171 [101] H. Chen, L. Qian, Z. Ma, W. Bai, Y. Li, D. Causon, C. Mingham, Application of an  
1172 overset mesh based numerical wave tank for modelling realistic free-surface  
1173 hydrodynamic problems, *Ocean Engineering*. 176 (2019) 97–117.

1174 [102] D.D. Chandar, On overset interpolation strategies and conservation on unstructured grids  
1175 in openfoam, *Computer Physics Communications*. 239 (2019) 72–83.

1176 [103] T. Wu, W. Luo, D. Jiang, R. Deng, S. Huang, Numerical Study on Wave-Ice Interaction  
1177 in the Marginal Ice Zone, *Journal of Marine Science and Engineering*. 9 (2021) 4.

1178 [104] C. Windt, J. Davidson, B. Akram, J.V. Ringwood, Performance assessment of the overset  
1179 grid method for numerical wave tank experiments in the OpenFOAM environment, in:  
1180 International Conference on Offshore Mechanics and Arctic Engineering, American  
1181 Society of Mechanical Engineers, 2018: p. V010T09A006.

1182 [105] C. Windt, J. Davidson, E.J. Ransley, D. Greaves, M. Jakobsen, M. Kramer, J.V.  
1183 Ringwood, Validation of a CFD-based numerical wave tank model for the power  
1184 production assessment of the wavestar ocean wave energy converter, *Renewable Energy*.  
1185 146 (2020) 2499–2516.

1186 [106] J.R. Chaplin, V. Heller, F.J.M. Farley, G.E. Hearn, R.C.T. Rainey, Laboratory testing the  
1187 Anaconda, *Philosophical Transactions of the Royal Society A: Mathematical, Physical  
1188 and Engineering Sciences*. 370 (2012) 403–424.

1189 [107] L. Huang, Y. Li, Design of the submerged horizontal plate breakwater using a fully  
1190 coupled hydroelastic approach, *Computer-Aided Civil and Infrastructure Engineering*. 37  
1191 (2022) 915–932. <https://doi.org/10.1111/mice.12784>.

1192 [108] L. Huang, K. Ren, M. Li, Ž. Tuković, P. Cardiff, G. Thomas, Fluid-structure interaction  
1193 of a large ice sheet in waves, *Ocean Engineering*. 182 (2019) 102–111.

1194 [109] N.G. Jacobsen, W. Bakker, W.S. Uijtewaal, R. Uittenbogaard, Experimental  
1195 investigation of the wave-induced motion of and force distribution along a flexible stem,  
1196 *Journal of Fluid Mechanics*. 880 (2019) 1036–1069.

1197 [110] M. Masoomi, A. Mosavi, The One-Way FSI Method Based on RANS-FEM for the Open  
1198 Water Test of a Marine Propeller at the Different Loading Conditions, *Journal of Marine  
1199 Science and Engineering*. 9 (2021) 351.

1200 [111] H. Chen, Q. Zou, Z. Liu, A coupled RANS-VOF and finite element model for wave  
1201 interaction with highly flexible vegetation, *COASTAL ENGINEERING*. (2016) 2.

1202 [112] A. Karac, Drop impact of fluid-filled polyethylene containers, PhD Thesis, Imperial  
1203 College London (University of London), 2003.

1204 [113] C.-G. Giannopapa, Fluid structure interaction in flexible vessels, PhD Thesis, University  
1205 of London, 2004.

1206 [114] C.J. Greenshields, H.G. Weller, A unified formulation for continuum mechanics applied  
1207 to fluid–structure interaction in flexible tubes, *International Journal for Numerical  
1208 Methods in Engineering*. 64 (2005) 1575–1593.

1209 [115] Z. Tukovic, H. Jasak, Updated Lagrangian finite volume solver for large deformation  
1210 dynamic response of elastic body, *Transactions of FAMENA*. 31 (2007) 55.

1211 [116] Z. Tukovic, P. Cardiff, A. Karac, H. Jasak, A. Ivankovic, OpenFOAM library for fluid  
1212 structure interaction, in: 9th OpenFOAM Workshop, 2014.

1213 [117] Ž. Tuković, A. Ivanković, A. Karač, Finite-volume stress analysis in multi-material linear  
1214 elastic body, *International Journal for Numerical Methods in Engineering*. 93 (2013) 400–  
1215 419.

1216 [118] J. McVicar, J. Lavroff, M.R. Davis, G. Thomas, Fluid–structure interaction simulation of  
1217 slam-induced bending in large high-speed wave-piercing catamarans, *Journal of Fluids  
1218 and Structures*. 82 (2018) 35–58.

1219 [119] L. Huang, An opensource solver for wave-induced FSI problems, In *Proceedings of CFD  
1220 with OpenSource Software*. Edited by Nilsson. H. (2018).  
1221 [http://dx.doi.org/10.17196/OS\\_CFD#YEAR\\_2017](http://dx.doi.org/10.17196/OS_CFD#YEAR_2017).

1222 [120] P. Cardiff, A. Karač, P. De Jaeger, H. Jasak, J. Nagy, A. Ivanković, Ž. Tuković, An open-  
1223 source finite volume toolbox for solid mechanics and fluid-solid interaction simulations,

- 1224 ArXiv Preprint ArXiv:1808.10736. (2018).
- 1225 [121] T. Tang, O. Hededal, P. Cardiff, On finite volume method implementation of poro-elasto-  
1226 plasticity soil model, *International Journal for Numerical and Analytical Methods in*  
1227 *Geomechanics*. 39 (2015) 1410–1430.
- 1228 [122] I. Oliveira, J. Gasche, P. Cardiff, Implementation and numerical verification of an  
1229 incompressible three-parameter Mooney-Rivlin model for large deformation of soft  
1230 tissues, in: *The 15th OpenFOAM Workshop*, 2020.
- 1231 [123] M. Girfoglio, A. Quaini, G. Rozza, Fluid-structure interaction simulations with a LES  
1232 filtering approach in solids4Foam, *ArXiv Preprint ArXiv:2102.08011*. (2021).
- 1233 [124] M. Abusara, N. Hakan, P. Cardiff, D. Randstrom, Fluid-structure interaction on a fixed  
1234 fan blade, in: *The 16th OpenFOAM Workshop*, 2021.
- 1235 [125] Y. Li, Z. Hu, L. Huang, Hydroelastic Simulation of Breaking Wave Impact on a Flexible  
1236 Coastal Seawall, in: *The 41th International Conference on Ocean, Offshore & Arctic*  
1237 *Engineering (OMAE)*, ASME: The American Society of Mechanical Engineers, 2022.
- 1238 [126] I.J. Losada, J.L. Lara, M. del Jesus, Modeling the interaction of water waves with porous  
1239 coastal structures, *Journal of Waterway, Port, Coastal, and Ocean Engineering*. 142 (2016)  
1240 03116003.
- 1241 [127] F. Mentzoni, T. Kristiansen, A Semi-Analytical Method for Calculating the  
1242 Hydrodynamic Force on Perforated Plates in Oscillating Flow, in: *International*  
1243 *Conference on Offshore Mechanics and Arctic Engineering*, American Society of  
1244 Mechanical Engineers, 2019: p. V07AT06A015.
- 1245 [128] A. George, I.H. Cho, Anti-sloshing effects of a vertical porous baffle in a rolling  
1246 rectangular tank, *Ocean Engineering*. 214 (2020) 107871.
- 1247 [129] S.K. Poguluri, I.H. Cho, Liquid sloshing in a rectangular tank with vertical slotted porous  
1248 screen: based on analytical, numerical, and experimental approach, *Ocean Engineering*.  
1249 189 (2019) 106373.
- 1250 [130] K. Shim, P. Klebert, A. Fredheim, Numerical investigation of the flow through and  
1251 around a net cage, in: *International Conference on Offshore Mechanics and Arctic*  
1252 *Engineering*, 2009: pp. 581–587.
- 1253 [131] H. Chen, E.D. Christensen, Investigations on the porous resistance coefficients for fishing  
1254 net structures, *Journal of Fluids and Structures*. 65 (2016) 76–107.
- 1255 [132] A. Feichtner, E. Mackay, G. Tabor, P.R. Thies, L. Johanning, D. Ning, Using a porous-  
1256 media approach for CFD modelling of wave interaction with thin perforated structures,  
1257 *Journal of Ocean Engineering and Marine Energy*. 7 (2021) 1–23.
- 1258 [133] S. Hadadpour, M. Paul, H. Oumeraci, Numerical investigation of wave attenuation by  
1259 rigid vegetation based on a porous media approach, *Journal of Coastal Research*. 92 (2019)  
1260 92–100.
- 1261 [134] P. Higuera, J.L. Lara, I.J. Losada, Three-dimensional interaction of waves and porous  
1262 coastal structures using OpenFOAM®. Part I: Formulation and validation, *Coastal*  
1263 *Engineering*. 83 (2014) 243–258.
- 1264 [135] P. Higuera, J.L. Lara, I.J. Losada, Three-dimensional interaction of waves and porous  
1265 coastal structures using OpenFOAM®. Part II: Application, *Coastal Engineering*. 83  
1266 (2014) 259–270.
- 1267 [136] M. Maza, J.L. Lara, I.J. Losada, Tsunami wave interaction with mangrove forests: A 3-D  
1268 numerical approach, *Coastal Engineering*. 98 (2015) 33–54.
- 1269 [137] A. Feichtner, E. Mackay, G. Tabor, P.R. Thies, L. Johanning, Comparison of Macro-  
1270 Scale Porosity Implementations for CFD Modelling of Wave Interaction with Thin  
1271 Porous Structures, *Journal of Marine Science and Engineering*. 9 (2021) 150.
- 1272 [138] B. Jensen, N.G. Jacobsen, E.D. Christensen, Investigations on the porous media equations  
1273 and resistance coefficients for coastal structures, *Coastal Engineering*. 84 (2014) 56–72.
- 1274 [139] N.G. Jacobsen, D.R. Fuhrman, J. Fredsøe, A wave generation toolbox for the open-source  
1275 CFD library: OpenFoam®, *International Journal for Numerical Methods in Fluids*. 70  
1276 (2012) 1073–1088.
- 1277 [140] A. Feichtner, E. Mackay, G. Tabor, P.R. Thies, L. Johanning, Modelling wave interaction

1278 with thin porous structures using OpenFOAM, in: Proceedings of the 13th European  
1279 Wave and Tidal Energy Conference (EWTEC 2019), Napoli, Italy, 2019: pp. 1–6.

1280 [141] A. Romano, J. Lara, G. Barajas, B. Di Paolo, G. Bellotti, M. Di Risio, I. Losada, P. De  
1281 Girolamo, Numerical modelling of Landslide-Generated Tsunamis with OpenFOAM®:  
1282 a new approach, *Coastal Structures 2019*. (2019) 486–495.

1283 [142] A. Feichtner, G. Tabor, E. Mackay, P. Thies, L. Johanning, On the use of a porous-media  
1284 approach for the modelling of wave interaction with thin perforated cylinders, in: *The  
1285 15th OpenFOAM Workshop (OFW15)*, Online, 2020.

1286 [143] P. Lin, Numerical modeling of breaking waves, PhD thesis, Cornell University, 1998.

1287 [144] P.L.-F. Liu, P. Lin, K.-A. Chang, T. Sakakiyama, Numerical modeling of wave  
1288 interaction with porous structures, *Journal of Waterway, Port, Coastal, and Ocean  
1289 Engineering*. 125 (1999) 322–330.

1290 [145] Y.-T. Wu, S.-C. Hsiao, Propagation of solitary waves over a submerged slotted barrier,  
1291 *Journal of Marine Science and Engineering*. 8 (2020) 419.

1292 [146] K.-H. Lee, J.-H. Bae, S.-G. Kim, D.-S. Kim, Three-dimensional simulation of wave  
1293 reflection and pressure acting on circular perforated caisson breakwater by OLAFOAM,  
1294 *Journal of Korean Society of Coastal and Ocean Engineers*. 29 (2017) 286–304.

1295 [147] V.K. Srineash, A. Kamath, K. Murali, H. Bihs, Numerical Simulation of Wave Interaction  
1296 with Submerged Porous Structures and Application for Coastal Resilience, *Journal of  
1297 Coastal Research*. 36 (2020) 752–770.

1298 [148] M. Brito, J. Fernandes, J.B. Leal, Porous media approach for RANS simulation of  
1299 compound open-channel flows with submerged vegetated floodplains, *Environmental  
1300 Fluid Mechanics*. 16 (2016) 1247–1266.

1301 [149] Y.-P. Zhao, C.-W. Bi, Y.-X. Liu, G.-H. Dong, F.-K. Gui, Numerical simulation of  
1302 interaction between waves and net panel using porous media model, *Engineering  
1303 Applications of Computational Fluid Mechanics*. 8 (2014) 116–126.

1304 [150] J. Chauchat, Z. Cheng, T. Nagel, C. Bonamy, T.-J. Hsu, SedFoam-2.0: a 3-D two-phase  
1305 flow numerical model for sediment transport, *Geoscientific Model Development*. 10  
1306 (2017) 4367–4392.

1307 [151] X. Liu, M.H. García, R. Muscari, Numerical investigation of seabed response under  
1308 waves with free-surface water flow, *International Journal of Offshore and Polar  
1309 Engineering*. 17 (2007).

1310 [152] M.A. Biot, General theory of three-dimensional consolidation, *Journal of Applied Physics*.  
1311 12 (1941) 155–164.

1312 [153] T. Tang, B. Johannesson, An integrated FVM simulation of wave-seabed-structure  
1313 interaction using OpenFoam, in: *9th OpenFOAM Workshop, 23-26 June 2014 in Zagreb,  
1314 Croatia, 2014*.

1315 [154] Y. Li, M.C. Ong, T. Tang, A numerical toolbox for wave-induced seabed response  
1316 analysis around marine structures in the OpenFOAM® framework, *Ocean Engineering*.  
1317 195 (2020) 106678.

1318 [155] Z. Lin, D. Pokrajac, Y. Guo, D. Jeng, T. Tang, N. Rey, J. Zheng, J. Zhang, Investigation  
1319 of nonlinear wave-induced seabed response around mono-pile foundation, *Coastal  
1320 Engineering*. 121 (2017) 197–211.

1321 [156] D. Celli, Y. Li, M.C. Ong, M. Di Risio, The role of submerged berms on the momentary  
1322 liquefaction around conventional rubble mound breakwaters, *Applied Ocean Research*.  
1323 85 (2019) 1–11.

1324 [157] D. Celli, Y. Li, M.C. Ong, M. Di Risio, Random wave-induced momentary liquefaction  
1325 around rubble mound breakwaters with submerged berms, *Journal of Marine Science and  
1326 Engineering*. 8 (2020) 338.

1327 [158] Z. Liang, D.-S. Jeng, PORO-FSSI-FOAM model for seafloor liquefaction around a  
1328 pipeline under combined random wave and current loading, *Applied Ocean Research*. 107  
1329 (2021) 102497.

1330 [159] J. Ye, K. He, L. Zhou, Subsidence prediction of a rubble mound breakwater at Yantai  
1331 port: A application of FSSI-CAS 2D, *Ocean Engineering*. 219 (2021) 108349.

- 1332 [160] H. Elsafti, H. Oumeraci, A numerical hydro-geotechnical model for marine gravity  
1333 structures, *Computers and Geotechnics*. 79 (2016) 105–129.
- 1334 [161] R.K. Shanmugasundaram, H. Rusche, C. Windt, Ö. Kirca, M. Sumer, N. Goseberg,  
1335 Towards the Numerical Modelling of Residual Seabed Liquefaction Using OpenFOAM,  
1336 *OpenFOAM® Journal*. 2 (2022) 94–115.
- 1337 [162] European Marine Energy Centre (EMEC), WAVE DEVICES, (2020).  
1338 <http://www.emec.org.uk/marine-energy/wave-devices/>.
- 1339 [163] G. Giorgi, J. Ringwood, Consistency of viscous drag identification tests for wave energy  
1340 applications, in: *Proceedings of the 12th European Wave and Tidal Energy Conference*  
1341 *27th Aug-1st Sept 2017, European Wave and Tidal Energy Conference 2017*, 2017: pp.  
1342 1–8.
- 1343 [164] C. Windt, J. Davidson, D.D. Chandar, N. Faedo, J.V. Ringwood, Evaluation of the overset  
1344 grid method for control studies of wave energy converters in OpenFOAM numerical wave  
1345 tanks, *Journal of Ocean Engineering and Marine Energy*. 6 (2020) 55–70.
- 1346 [165] E.J. Ransley, D.M. Greaves, A. Raby, D. Simmonds, M.M. Jakobsen, M. Kramer, RANS-  
1347 VOF modelling of the Wavestar point absorber, *Renewable Energy*. 109 (2017) 49–65.  
1348 <https://doi.org/10.1016/j.renene.2017.02.079>.
- 1349 [166] J. Palm, C. Eskilsson, L. Bergdahl, R.E. Bensow, Assessment of Scale Effects, Viscous  
1350 Forces and Induced Drag on a Point-Absorbing Wave Energy Converter by CFD  
1351 Simulations, *Journal of Marine Science and Engineering*. 6 (2018) 124.  
1352 <https://doi.org/10.3390/jmse6040124>.
- 1353 [167] B.W. Schubert, F. Meng, N.Y. Sergiienko, W. Robertson, B.S. Cazzolato, M.H. Ghayesh,  
1354 A. Rafiee, B. Ding, M. Arjomandi, Pseudo-nonlinear hydrodynamic coefficients for  
1355 modelling point absorber wave energy converters, in: *Proceedings of the 4th Asian Wave*  
1356 *and Tidal Energy Conference, Taipei, Taiwan, 2018*: pp. 9–13.
- 1357 [168] F. Meng, A. Rafiee, B. Ding, B. Cazzolato, M. Arjomandi, Nonlinear hydrodynamics  
1358 analysis of a submerged spherical point absorber with asymmetric mass distribution,  
1359 *Renewable Energy*. 147 (2020) 1895–1908. <https://doi.org/10.1016/j.renene.2019.09.101>.
- 1360 [169] C. Windt, J. Davidson, J.V. Ringwood, Numerical analysis of the hydrodynamic scaling  
1361 effects for the Wavestar wave energy converter, *Journal of Fluids and Structures*. 105  
1362 (2021) 103328. <https://doi.org/10.1016/j.jfluidstructs.2021.103328>.
- 1363 [170] H. Akimoto, K. Tanaka, Y.Y. Kim, Drag-type cross-flow water turbine for capturing  
1364 energy from the orbital fluid motion in ocean wave, *Renewable Energy*. 76 (2015) 196–  
1365 203. <https://doi.org/10.1016/j.renene.2014.11.016>.
- 1366 [171] C. Xu, Z. Huang, Three-dimensional CFD simulation of a circular OWC with a nonlinear  
1367 power-takeoff: Model validation and a discussion on resonant sloshing inside the  
1368 pneumatic chamber, *Ocean Engineering*. 176 (2019) 184–198.  
1369 <https://doi.org/10.1016/j.oceaneng.2019.02.010>.
- 1370 [172] A. Iturrioz, R. Guanache, J.L. Lara, C. Vidal, I.J. Losada, Validation of OpenFOAM® for  
1371 Oscillating Water Column three-dimensional modeling, *Ocean Engineering*. 107 (2015)  
1372 222–236. <https://doi.org/10.1016/j.oceaneng.2015.07.051>.
- 1373 [173] Z. Deng, C. Wang, P. Wang, P. Higuera, R. Wang, Hydrodynamic performance of an  
1374 offshore-stationary OWC device with a horizontal bottom plate: Experimental and  
1375 numerical study, *Energy*. 187 (2019) 115941.  
1376 <https://doi.org/10.1016/j.energy.2019.115941>.
- 1377 [174] A. Dimakopoulos, M. Cooker, E. Medina-Lopez, D. Longo, R. Pinguet, Flow  
1378 characterisation and numerical modelling of owc wave energy converters, in: *11th*  
1379 *European Wave & Tidal Energy Conference (EWTEC)*. Nantes, France, 2015.
- 1380 [175] J. Gadelho, C.G. Soares, G. Barajas, J.L. Lara, CFD analysis of the PTO damping on the  
1381 performance of an onshore dual chamber OWC, *Trends in Maritime Technology and*  
1382 *Engineering Volume 2*. (2022) 381–389.
- 1383 [176] K. Rezanejad, J.F.M. Gadelho, C. Guedes Soares, Hydrodynamic analysis of an  
1384 oscillating water column wave energy converter in the stepped bottom condition using  
1385 CFD, *Renewable Energy*. 135 (2019) 1241–1259.

1386 <https://doi.org/10.1016/j.renene.2018.09.034>.

1387 [177] I. Simonetti, L. Cappiotti, H. El Safti, H. Oumeraci, Numerical modelling of fixed  
1388 oscillating water column wave energy conversion devices: Toward geometry hydraulic  
1389 optimization, in: International Conference on Offshore Mechanics and Arctic  
1390 Engineering, American Society of Mechanical Engineers, 2015: p. V009T09A031.

1391 [178] I. Simonetti, L. Cappiotti, H. Elsafti, H. Oumeraci, Optimization of the geometry and the  
1392 turbine induced damping for fixed detached and asymmetric OWC devices: A numerical  
1393 study, *Energy*. 139 (2017) 1197–1209. <https://doi.org/10.1016/j.energy.2017.08.033>.

1394 [179] T.T. Loh, D. Greaves, T. Maeki, M. Vuorinen, D. Simmonds, A. Kyte, Numerical  
1395 modelling of the WaveRoller device using OpenFOAM, in: Proceedings of the 3rd Asian  
1396 Wave & Tidal Energy Conference, 2016.

1397 [180] J.A. Bridgwater Court, D.R.S. Cahndel, A.R. Plummer, A.J. Hillis, Modelling of array  
1398 interactions for a curved OSWEC using OpenFOAM, in: The 12th European Wave and  
1399 Tidal Energy Conference (EWTEC), Cork, 2017.

1400 [181] L. Chen, L. Sun, J. Zang, A.J. Hillis, A.R. Plummer, Numerical study of roll motion of a  
1401 2-D floating structure in viscous flow, *Journal of Hydrodynamics, Ser. B*. 28 (2016) 544–  
1402 563.

1403 [182] E. Renzi, S. Michele, S. Zheng, S. Jin, D. Greaves, Niche applications and flexible devices  
1404 for wave energy conversion: A review, *Energies*. 14 (2021) 6537.

1405 [183] I. Collins, M. Hossain, W. Dettmer, I. Masters, Flexible membrane structures for wave  
1406 energy harvesting: A review of the developments, materials and computational modelling  
1407 approaches, *Renewable and Sustainable Energy Reviews*. 151 (2021) 111478.

1408 [184] L. Huang, Z. Hu, Y. Li, G. Thomas, Fully-coupled CFD+CSM analysis on an elastic  
1409 floating/submerged plate for wave energy harvest, in: 9th International Conference on  
1410 HYDROELASTICITY IN MARINE TECHNOLOGY, Rome, Italy, 2022.

1411 [185] A. Rafiee, J. Fiévez, Numerical prediction of extreme loads on the CETO wave energy  
1412 converter, in: Proceedings of the 11th European Wave and Tidal Energy Conference,  
1413 Nantes, France, 2015.

1414 [186] M. Penalba, J. Davidson, C. Windt, J.V. Ringwood, A high-fidelity wave-to-wire  
1415 simulation platform for wave energy converters: Coupled numerical wave tank and power  
1416 take-off models, *Applied Energy*. 226 (2018) 655–669.  
1417 <https://doi.org/10.1016/j.apenergy.2018.06.008>.

1418 [187] C. Jiang, O. el Moctar, G. Moura Paredes, T.E. Schellin, Validation of a dynamic mooring  
1419 model coupled with a RANS solver, *Marine Structures*. 72 (2020) 102783.  
1420 <https://doi.org/10.1016/j.marstruc.2020.102783>.

1421 [188] J. Palm, C. Eskilsson, MOODY User Manual: version 1.0. 0, (2018).

1422 [189] M. Hall, Moordyn v2: New capabilities in mooring system components and load cases,  
1423 in: International Conference on Offshore Mechanics and Arctic Engineering, American  
1424 Society of Mechanical Engineers, 2020: p. V009T09A078.

1425 [190] H. Chen, M. Hall, CFD simulation of floating body motion with mooring dynamics:  
1426 Coupling MoorDyn with OpenFOAM, *Applied Ocean Research*. 124 (2022) 103210.

1427 [191] J. Palm, C. Eskilsson, L. Bergdahl, An hp-adaptive discontinuous Galerkin method for  
1428 modelling snap loads in mooring cables, *Ocean Engineering*. 144 (2017) 266–276.

1429 [192] G. Barajas, J.L. Lara, B. Di Paolo, I.J. Losada, Analysis of a floating wave energy  
1430 converter interaction with waves using the Overset framework, in: The 9th Conference  
1431 on Computational Methods in Marine Engineering (Marine 2021), 2022.

1432